OPTIMIZATION OF A 48 ECHO MAGNETIC RESONANCE IMAGING SEQUENCE USING VARIABLE TR DATA ACQUISITION

Cornelia Laule

B.Sc. (Physics) University of British Columbia, 1999

A THESIS SUBMITTED IN PARTIAL FULFILLMENT OF

THE REQUIREMENTS FOR THE DEGREE OF

MASTER OF SCIENCE

in

THE FACULTY OF GRADUATE STUDIES

DEPARTMENT OF PHYSICS

We accept this thesis as conforming

to the required standard

THE UNIVERSITY OF BRITISH COLUMBIA

December 2000

In presenting this thesis in partial fulfilment of the requirements for an advanced degree at the University of British Columbia, I agree that the Library shall make it freely available for reference and study. I further agree that permission for extensive copying of this thesis for scholarly purposes may be granted by the head of my department or by his or her representatives. It is understood that copying or publication of this thesis for financial gain shall not be allowed without my written permission.

Department of Physics

The University of British Columbia
Vancouver, Canada

Date Dec 15, 2000

DE-6 (2/88)

Abstract

Magnetic resonance imaging (MRI) is a very valuable tool for studying the brain. Currently, MRI is the only non-invasive method for investigating myelin. A unique MRI pulse sequence which is used to investigate myelin is a 48 echo CPMG experiment with TR = 3800ms and TE 10 and 50ms. Unfortunately, this experiment takes over 33 minutes to complete, making clinically less feasible to use. By collecting higher order regions of k-space at shorter TR times, the experiment can be shortened, but at a cost of increasing image blurrines and at a potential loss of data. The purpose of this thesis was to investigate collecting different regions of k-space at different TR times in order to try and optimize a new 48 echo variable TR pulse sequence.

Simulations were first performed using five spin-echo images with different TR. By creating simulated variable TR images, we were able to qualitatively investigate the resulting blurriness of the images. Visual assesment of the created images and the difference images allowed us to determine what degree of resolution deterioration would still allow us to differentiate between important structures. It was decided that the simulation for 60 out of 128 lines collected at a shorter TR had the optimal decrease in scan time, without too great a compromise in image quality. The variable TR CPMG experiment was then run on 9 phantoms with different T_1 and T_2 relaxation times. By studying samples with known T_1 and T_2 relaxation times, we were able to investigate the reliability of the variable TR pulse sequence. Comparing decay curves showed no difference between 0 and 100 lines of k-space collected at a shorter TR – it was only when all 128 lines of k-space were collected at the shorter TR that a decrease in amplitude of the decay curve occurred. Experiments showed that proton density, GMT2 and chi squared of the T_2 decay curve fit for the phantoms were unaffected up to and including 100 lines of k-space collected at TR of 2120ms. Finally, *in-vivo* studies were performed on five volunteers. Comparing the difference in decay curves, proton density and geometric mean T_2 showed only very minor differences between data collected using the constant TR sequence and data collected using the variable TR program in which 60 out of 128 k–space lines were collected at a shorter TR of 2120ms. Experiments showed small differences in myelin water fraction, which could be explained by ROI's being drawn slightly different on the constant and variable images. The chi squared was less for the variable TR, which could be caused by smoothing introduced when collecting different k-space lines at different TR's.

Table of Contents

List of Tables

List of Figures

Acknowledgements

It's 6:54am and I am sitting in Muffin Break, trying to prioratize all those to whom I am indebted to for helping me with this degree. Without a doubt, the most important person has been Alex. Thank you for believing in me. Thank you for all your support. You are so much more than a supervisor. You are a role model and a friend. Thank you Ken for being a constant source of knowledge, for answering all my questions and coming to my rescue more than once. (I will master PV-WAVE yet !). Thank you Irene for your help and insite. You're an awesome friend and another great role model. Here's to early morning bike rides ! Thank you Burkie for coffee, cookies, lunch, more coffee, dinner, helping me improve my vocabulary and trusting me with your car. Thank you Sofia, Greg and Mateo for your friendship and reminding me what's important. Thank you San for reading this thesis on such short notice. You have taught me a lot and I look forward to learning more from you. Thank you Neil for giving me a chance – I will be forever indebted to you. Also, thank you for having really great Christmas parties. Thank you all my volunteers, especially Karen, and thank you Steve for being a great friend and letting me be me. Thanks to Elana, Bernice, Charmaine, Carolyn, Evan, Matt, Rachel, Phil and Drew (aka foozball champion) for making room 100 a much brighter (and louder) place this summer and fall. Any last, but certainly not least, thank you to the MS Society of Canada for funding me to do this research and allowing me to begin my career as an academic.

Chapter 1

Introduction

1.1 Brain and Myelin

The central nervous system (CNS) contains 10^{12} special cells called neurons which facillitate the transmission of electrical signals from one location in the body to another. The transmission of such signals is what allows us to function. The CNS can be divided into grey matter and white matter. The grey matter contains the cell bodies of neurons, while the white matter contains the nerve fibers which actually transport signals. What gives the white matter it's distinctive coloring is the insulating layer which surrounds it: *myelin*. Myelin is made up of a 80% lipid and 20% protein bilayer which wraps itself around the axon of neurons. See Figure 1.1

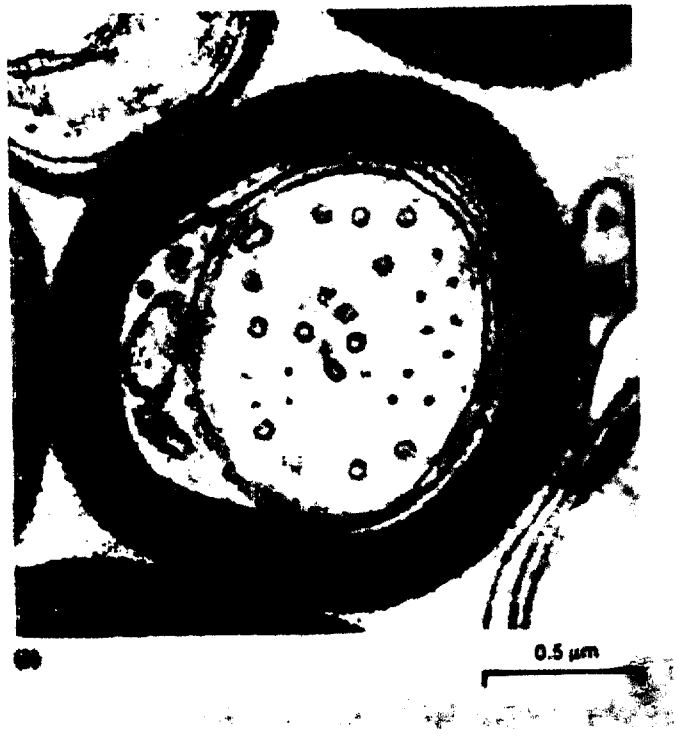

Figure 1.1 Myelin sheaths wrapped around axon [1]

This insulating layer acts to speed up the velocity of signal transmission by ten to one hundred times. Myelin is of critical importance because speed is fundamental in sending signals around our body. Without myelin it would take much longer for a signal to get from our brain to our extremties, resulting in slower reaction time. This is because sodium-potassium channels which propagate the nerve signals would have to be placed all along the nerve fiber, instead of just at places with no myelin, or nodes. Figure 1.2 shows a schematic of the breakdown of the human brain.

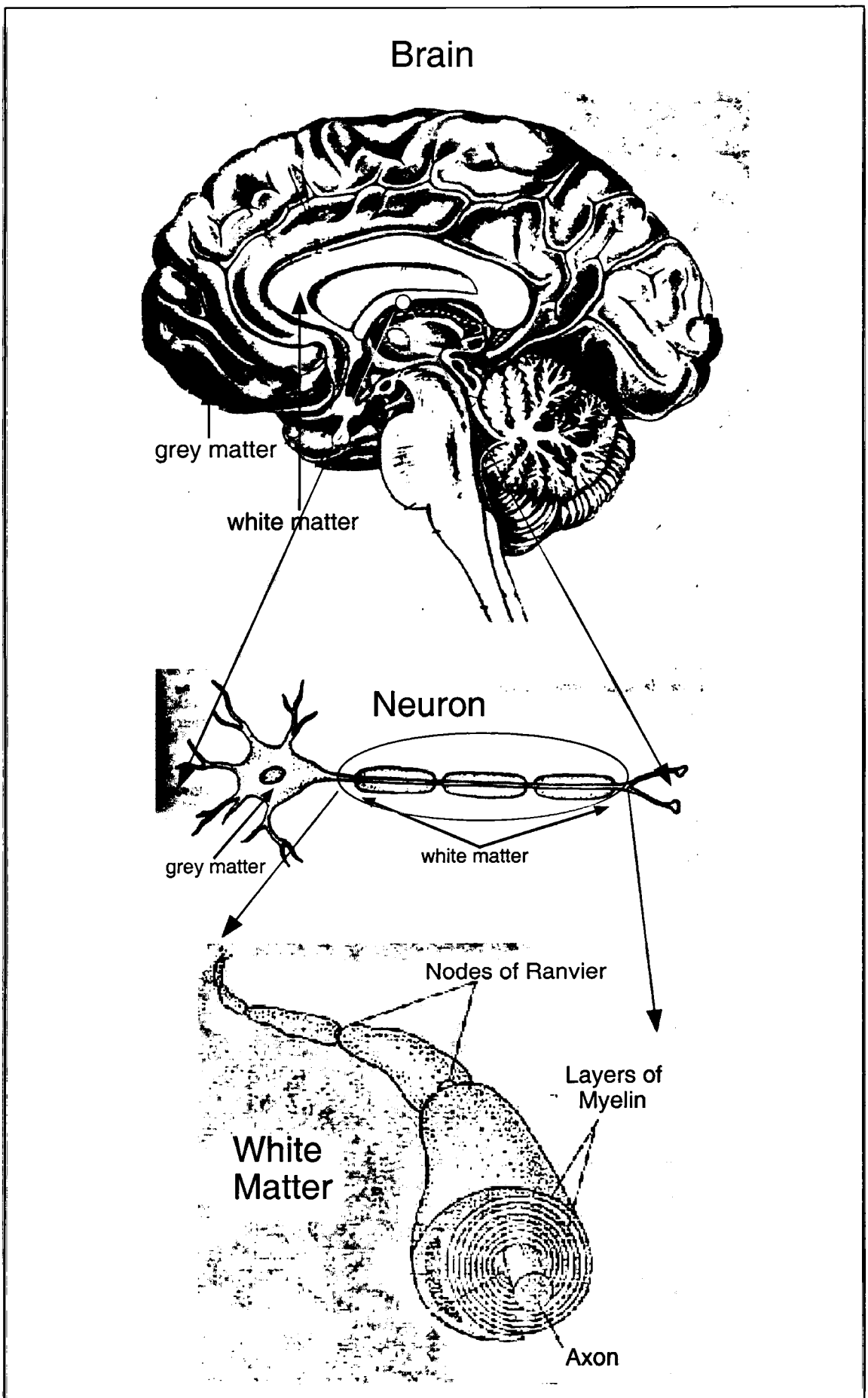

Figure 1.2 White and grey matter in brain

An electron micrograph of a neuron is shown in Figure 1.3 and 1.4 The myelin is not a continuous coating over the axon - there are discontinuities called Nodes of Ranvier. It is these discontinuities which allow the conduction signal to propagate at a much faster rate.

Figure 1.3 Electron micrograph of a neuron [2]

Figure 1.4 Electron micrograph of a Node of Ranvier [3]

1.2 Multiple Sclerosis

Myelin plays an important role in signal transmission and there are many different myelin related diseases. One such disease is multiple sclerosis (MS). The disease of MS was first described in the 1830's. Two descriptions were published which described a disease which caused multiple areas of discoloration and shrinkage throughout the brain. [4] This is where the name multiple sclerosis, or many scars, originates. We have come a long way in the last century and a half, during which time many interpretations of the disease have been explored with the aid of diagnostic tools and many hypotheses concerning the pathogenesis of MS have come and gone.

Multiple Sclerosis (MS) is an inflammatory disease which is characterized by the destruction of the CNS myelin, which includes the brain, spinal cord and optic nerves. MS both promotes the removal of the myelin which forms the white matter in the CNS and also impairs the body's ability to repair the subsequent areas of demyelination. The hallmarks of MS include areas of demyelination, oligodendrocyte loss and axonal degeneration. Figure 1.5 shows nerve conduction in a partially demyelinated axon. The signal cannot propagate as quickly or efficiently through the portion where there is myelin degredation.

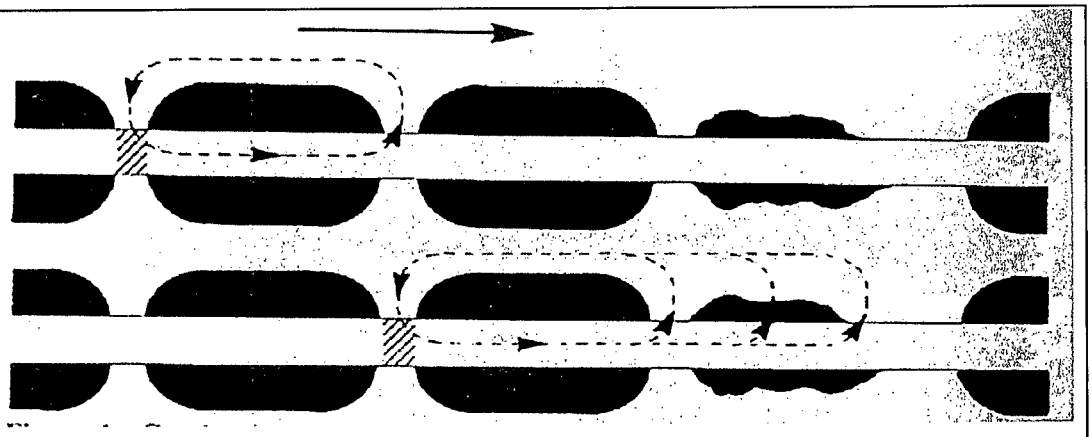

Figure 1.5 Nerve conduction in a normal portion (top) and a demyelinated portion (bottom) of the axon. In demyelinated region the action potential is diffused over a larger area, reducing conduction velocity. [1]

Over 50,000 Canadians suffer from this disease, with women being affected three times more often than men. People living in a cold climate have a higher likelihood of developing the disease than those residing in a warm climate. It has been shown that someone over the age of 15 moving from a cold climate to the tropics is much more likely to develop MS than a native of the warm climate. However, someone who emigrates to the tropics before the age of 15 is no more likely to develop MS than is a native. Genetics are also thought to play a factor in MS susceptibility [1]. In the last 20 years a powerful diagnostic tool has become clinically available to aid in the describing and diagnosing of multiple sclerosis: MRI.

1.3 Magnetic Resonance Imaging

1.3.1 Theory

The structure of the atom is such that it is made up of a nucleus surrounded by orbiting electrons. The nucleus is then made up of protons and neutrons. Certain atoms which have either an odd number of neutrons or protons have a non zero spin angular momentum **j**, as well as an associated magnetic moment **m**. A constant which can be derived from the ratio of the magnetic moment to the angular momentum is called the *gyromagnetic ratio*, or γ, and is specific to each atom.

$$\gamma = \frac{|\mathbf{m}|}{|\mathbf{j}|} \tag{1.1}$$

Some examples of nuclei with a non-zero spin angular momentum are ^{23}Na, ^{31}P, ^{39}K, ^{13}C, ^{15}N and ^{1}H. The hydrogen nucleus, sometimes simply referred to as the proton, is the nucleus which forms the basis of MRI. When these nuclei are not in the presence of an external magnetic field they are randomly oriented and the net angular momentum and magnetic moment of the system is zero. However, when these nuclei are placed in an

external magnetic field, **B**, the system becomes polarized and the net angular momentum and magnetic moment are no longer zero.

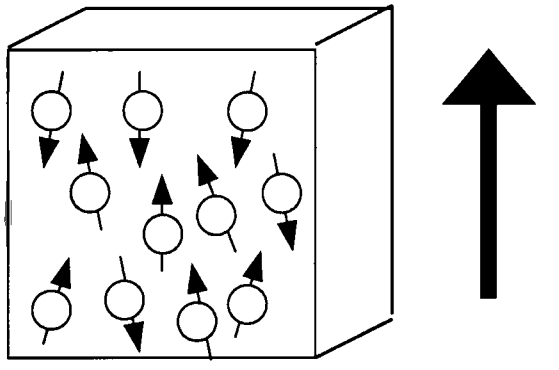

Figure 1.6 Nuclei orient either with or against external magnetic field [5]

Each nuclei rotates, like a spinning top, at a frequency called the *Larmor frequency*, which is given the symbol ω,

$$\omega = \gamma \mathbf{B} \tag{1.2}$$

The energy of a nucleus in an external magnetic field is given by

$$E = - \mathbf{m} \bullet B \tag{1.3}$$

From equation (1.1) we obtain the relation that $\mathbf{m} = \gamma \mathbf{j}$ and with the knowledge that

$$\mathbf{j} = \frac{hS}{2\pi} \tag{1.4}$$

we can define E as

$$E = -\frac{\gamma hS}{2\pi} \bullet \mathrm{B} \tag{1.5}$$

Since S = ± 1/2 for a particle with spin number s = 1/2, there are two (2s + 1) possible energy states and hence also this number of possible orientations in which the nuclei can exist while being acted upon by an external magnetic field.

From statistical mechanics we know that the probability of the nuclei being found in the two states is not equal. The Boltzmann distribution

$$\mathrm{P(E)} \propto \exp\left(-\frac{E}{kT}\right) \tag{1.6}$$

gives the probability of a nucleus being in a certain energy state. At a temperature of 300K and magnetic field of 1.5 T, the ratio between the upper (E-) and lower (E+) energy state populations is

$$R = \frac{P(E-)}{P(E+)} = \exp\left(\frac{\Delta E}{kT}\right) = \exp\left(\frac{\gamma hB}{2\pi kT}\right) \approx 1 + \left(\frac{\gamma hB}{2\pi kT}\right) = 1.000102$$

Because R is larger than one it can be concluded that there is a slight excess of nuclei in the lower energy state and as a result there is a non zero total magnetic moment **M** when the nuclei are placed in an external magnetic field [5]. Figure 1.10 shows this phenomenon, also known as Zeeman energy splitting.

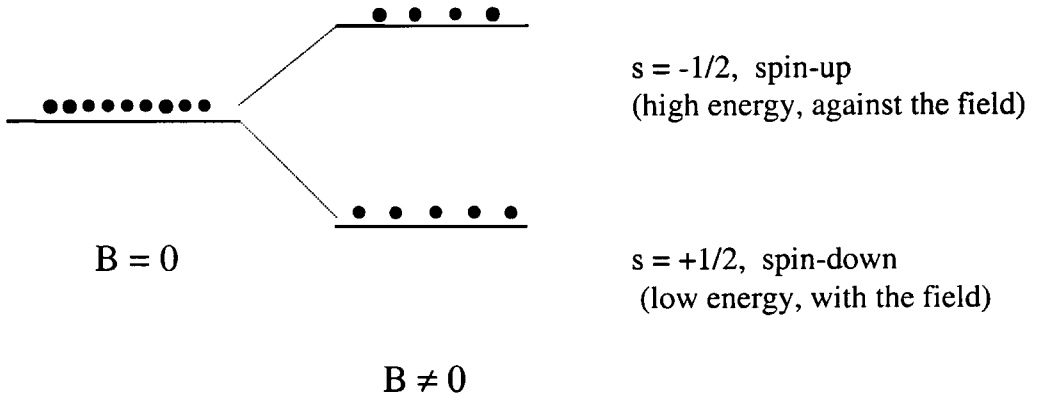

Figure 1.7 Zeeman energy splitting

1.3.2 MRI Signal Detection and Localization

For a group or an ensemble of nuclei in a certain volume, the equation of motion for the magnetization vector **M** (the sum of all the nuclei) is given by the Bloch equation

$$\frac{d}{dt}\mathbf{M} = \gamma \mathbf{M} \times \mathbf{B} - \frac{\mathbf{M}_X \hat{x} + \mathbf{M}_Y \hat{y}}{T_2} - \left(\frac{\mathbf{M}_Z - \mathbf{M}_O}{T_1}\right)\hat{z} \qquad (1.7)$$

The magnetic moment **m** for each nuclei is pointing either in the direction of the external field (low energy state) or against the direction of the external field (high energy state).

Since there is a slight excess of individual magnetization vectors pointing in the direction of the applied field, **M** will point also in this direction. When you tip **M** away from its equilibrium value of M_O this magnetization vector precesses, similar in motion to a tipped rotating top in a gravitational field. See figure 1.11 below.

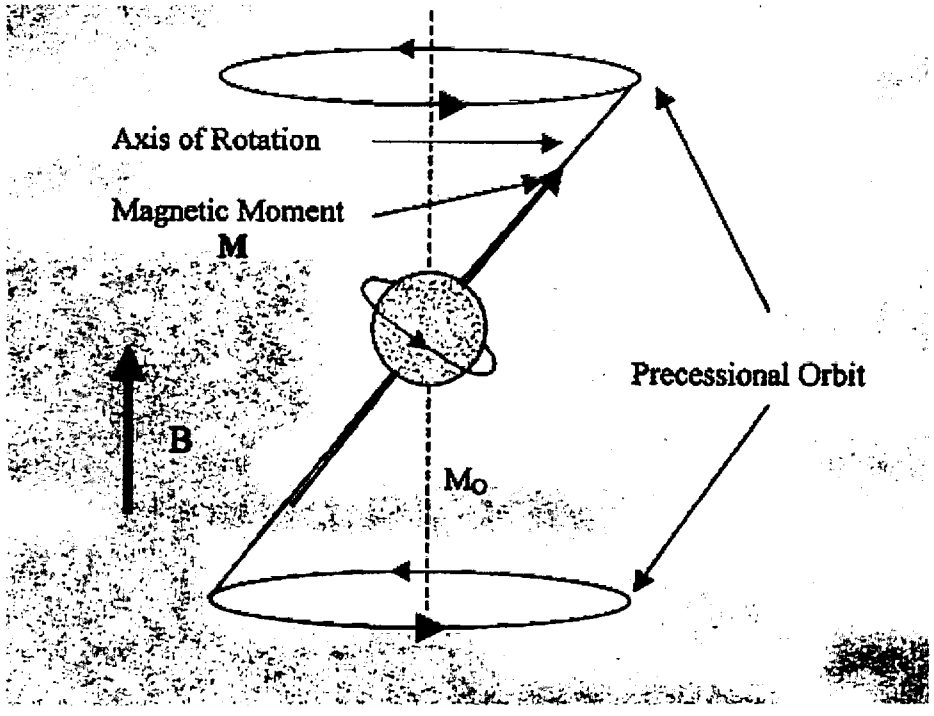

Figure 1.8 Precessing Nucleus - this individual nucleus represents the ensemble of all nuclei in the system. When **M** is tipped away fron equilibrium it is not the indivdual nuclei which tip, but rather some of the magnetic moments, **m**, which change from spin up to spin down and cause **M** to tip.

Eventually **M** will return to its thermal equilibrium value of M_O. This is called relaxation. There are two kinds of relaxation which contribute to the return of M to M_O. The first is called longitudinal relaxation or spin-lattice ($\mathbf{T_1}$) relaxation. This involves relaxation along B, towards M_O and is caused by interactions between the nucleus and the surrounding lattice. The second is called transverse relaxation or spin-spin ($\mathbf{T_2}$) relaxation. This involves relaxation perpendicular to B, towards zero and is caused by interactions between different nuclei.

In order to tip the magnetization vector away from M_O, an oscillating magnetic field placed perpendicular to the external field B_O and tuned to the Larmor frequency, is applied to the nuclei. Photons will be absorbed if this radio frequency (RF) is at the

Larmor frequency and nuclei will be excited from low to high energy. This is called RF excitation. It is important for the RF to be on resonance (i.e. at the Larmor frequency) because otherwise the RF has little effect. The angle the net magnetization is flipped is defined by

$$\theta = \gamma B_1 \tau \tag{1.8}$$

Both the duration of the RF pulse and the size of the amplitude determines the size of the flip angle. After the excitation occurs there can be a transverse component of the magnetization vector. This transverse component can be detected as an induction signal in a receiver coil placed around the patient due to the magnetic flux caused by the precession of the transverse magnetization. Even after the RF is turned off, **M** will continue to precess until it relaxes back to M_O via T_1 and T_2 relaxation. While this is happening a free induction decay signal or FID can be detected. (See Figure 1.12)

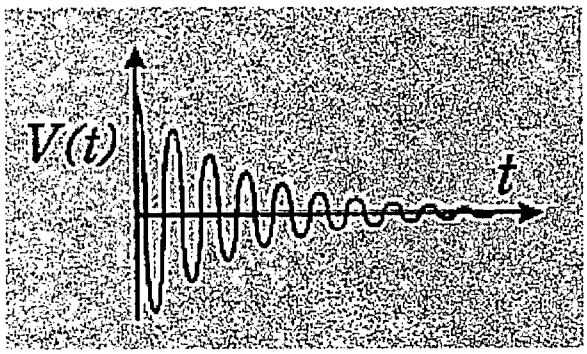

Figure 1.9 Free Induction Decay [5]

However, for the technique of MRI, simply receiving a signal from the entire body is useless. Ideally, we want to investigate a signal in a certain location and extract as much information as possible from it in order to create an accurate image representation. To do this, a successful MR imager must contain the following components: (a) Main

magnet which will provide the homogeneous magnetic field, (b) RF system for excitation and signal detection, (c) Gradient system made up of gradient amplifiers and coils (This component is very important because this is what links spatial location to the Larmor frequency of the nuclei), and (d) Computer to synchronize the actions of all the components.

The gradient system of the MR scanner allows the use of magnetic field gradients for the basis of three signal localization techniques - slice selection, frequency encoding and phase encoding.

Slice Selection - Selecting a particular slice is done by making the magnetic field vary from point to point in the patient's body by using a gradient coil. This makes each position have its own Larmor frequency and when the RF pulse with a bandwidth of frequencies is transmitted, only a certain portion or *slice* of the patient will be excited and send back an induction signal. Although such a slice selective gradient can be physically applied in any desired direction it is usually given the logical name Gz for convenience. This G_Z gradient is usually on when the RF is on, in order to excite the right slice.

Frequency Encoding - After the desired slice is selected we now need to obtain information about individual pixels within that slice when the induction signal is received. To get spatial information in the x direction of the slice, we apply another gradient, G_X, called the frequency encoding gradient. This G_X gradient is applied during the time the echo is received, i.e. during readout time.

Phase Encoding - In addition to obtaining magnitude information from each pixel in the selected slice, it is also possible to obtain direction or phase information for the individual induction signals. To obtain spatial information in the y direction, another gradient, G_Y , called the phase encoding gradient, is applied in the y direction. This magnetic field gradient in the y direction is turned on for a certain period of time between the slice

selection and frequency encoding, causing the nuclei at different Y positions to have different phases.

1.3.3 Pulse Sequences

In order for the computer component of the MR system to run, programs must be written which tell the computer what to do and when to do it. These programs are known as pulse sequences and can be pictorially represented, as shown in Figure 1.13

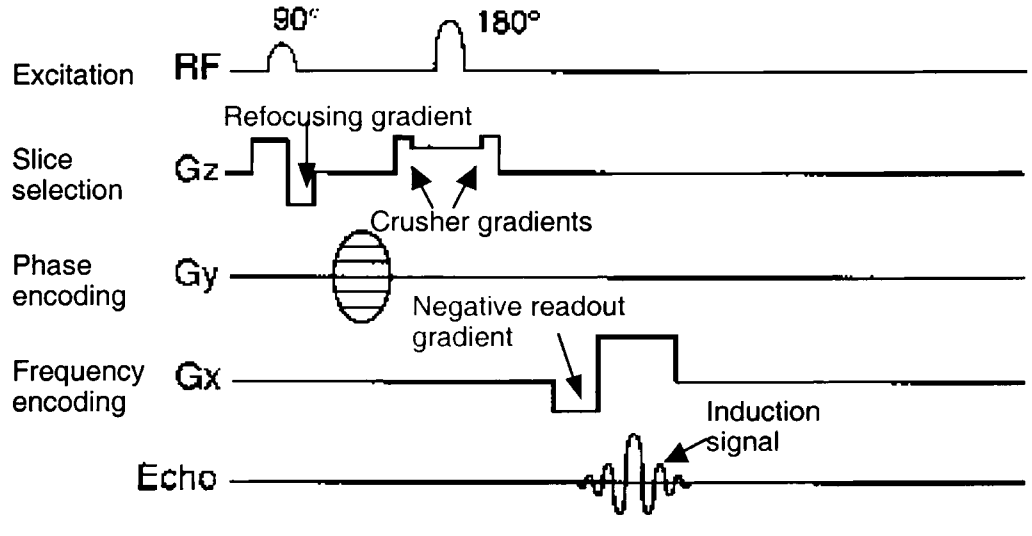

Figure 1.10 A spin echo pulse sequence diagram [6]

In this particular pulse sequence the RF excitation 90^{O} and 180^{O} pulses are simply Gaussian in nature. There are other possible shapes for the RF pulse, including the commonly used sinc function and rectangular pulse. The Fourier transform of the pulse shape gives the slice profile. The slice selective G_Z gradient is on during both the 90^{O} and 180^{O}. During the 90^{O} pulse there is first a positive gradient which selects the slice and

then a negative gradient which acts to rephase all of the spins in the slice select direction. Immediately before and after the 180^{O} pulse there are crusher gradients in place, which are applied to offset any error that may occur if the 180^{O} pulse is not exactly 180^{O}. These crusher gradients help eliminate stimulated echoes, as well as diminish signal from flow effects. At the time the FID or echo occurs and the data is collected, the G_X gradient is on. If a positive gradient were to be applied directly, everything would end up being dephased and decreased in signal. So instead, a gradient is first applied in the negative direction just before the echo occurs. This negative gradient has an area equal to half of that of the readout gradient (see Figure 1.14). Then, a positive gradient is applied such that the spins will rephase at the center of the pulse, corresponding to the midpoint of the echo, at time TE. The time from the original 90^{o} pulse until it is repeated is called time TR.

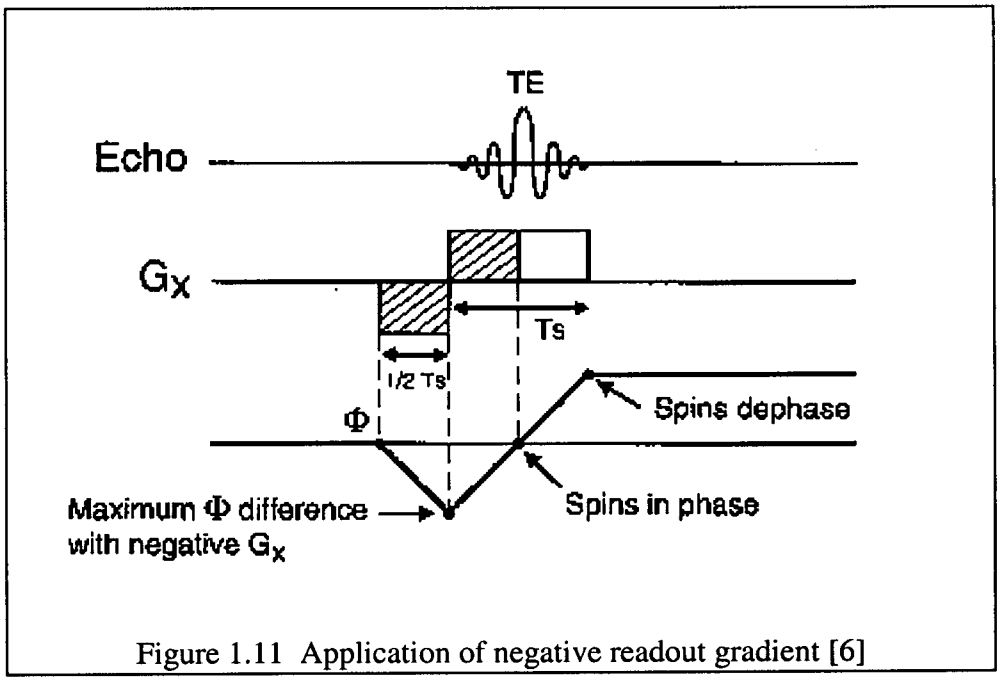

Figure 1.11 Application of negative readout gradient [6]

1.3.4 K-space and image reconstruction

The complex induction signal which is detected in MRI can be expressed as

$$S(k_x,k_y) = \iint M(x,y)e^{ixk_x}e^{iyk_y}dxdy \qquad (1.9)$$

where M(x, y) is the 2 dimensional distribution of the transverse magnetization and k_x and k_y are variables defined as

$$k_x = \gamma G_x t \qquad (1.10)$$

$$k_y = \gamma G_y T \qquad (1.11)$$

This 2 dimensional distribution of k_x and k_y is referred to as k-space. Figure 1.15 shows a map of k-space.

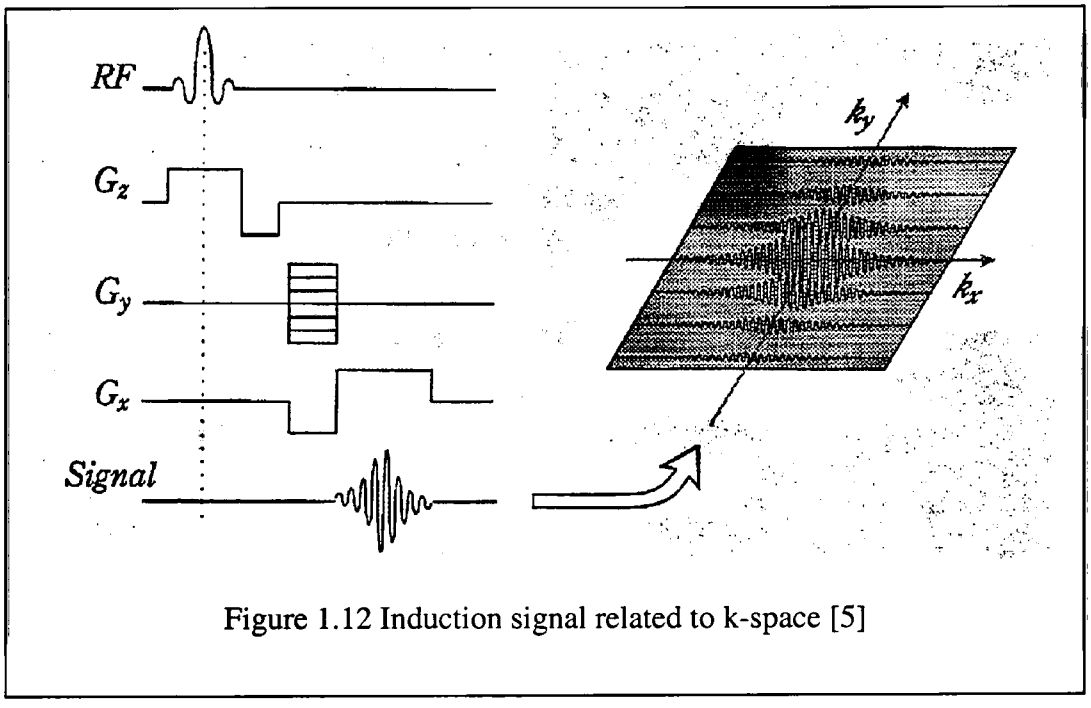

Figure 1.12 Induction signal related to k-space [5]

Once the entire set of data to fill all of k-space has been collected, a Fourier transform is applied to the data and changes it from frequency to image domain. The outer portions of

k-space (refered to as high order lines) correspond to fine detail, while the inner portion or low order k-space gives contrast. Figure 1.16 shows the significance of the different spatial frequency components.

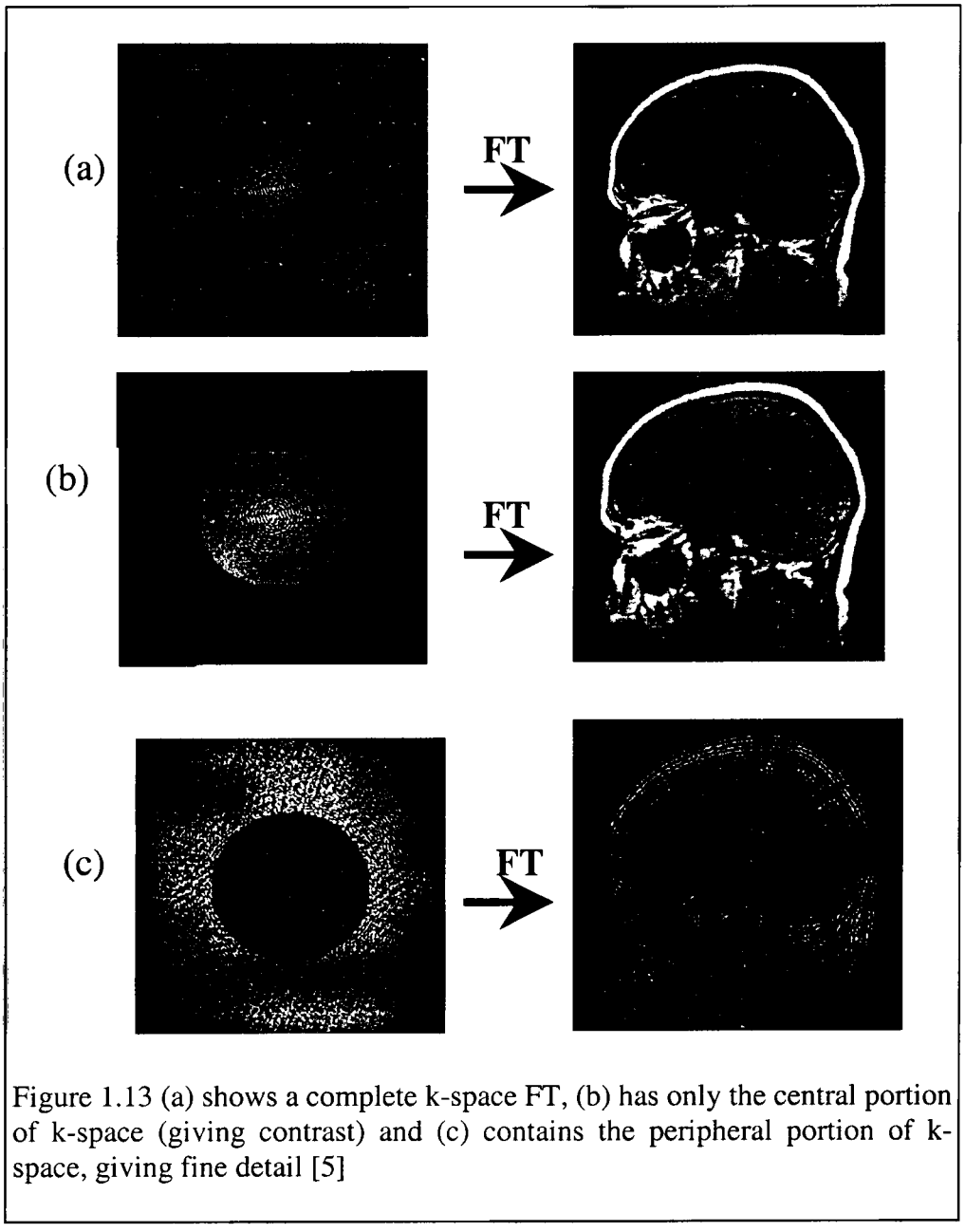

Figure 1.13 (a) shows a complete k-space FT, (b) has only the central portion of k-space (giving contrast) and (c) contains the peripheral portion of k-space, giving fine detail [5]

Chapter 2

General Methods

2.1 MRI Pulse Sequences

Many different quantities can be investigated with magnetic resonance imaging and as a result there are hundreds of different pulse sequences which have been invented.

2.1.1 General CPMG Experiment

To investigate the T_2 relaxation time, i.e. how fast the transverse component of magnetization relaxes towards zero, a spin echo pulse sequence is traditionally used. The sequence can be written as

$$90_x - \tau/2 - (180_y - \tau/2)_n$$

In this experiment, a 90° rf pulse is first applied along the x direction, tipping the magnetization from the positive z axis into the xy plane. The spins which make up the net magnetization begin to dephase and spread out. After a certain time $\tau/2$ a 180° pulse along the y direction is applied, causing the spins to flip by 180° and eventually rephase. Once the magnetization has completely rephased, an induction signal or echo is produced and detected. See figure 2.1

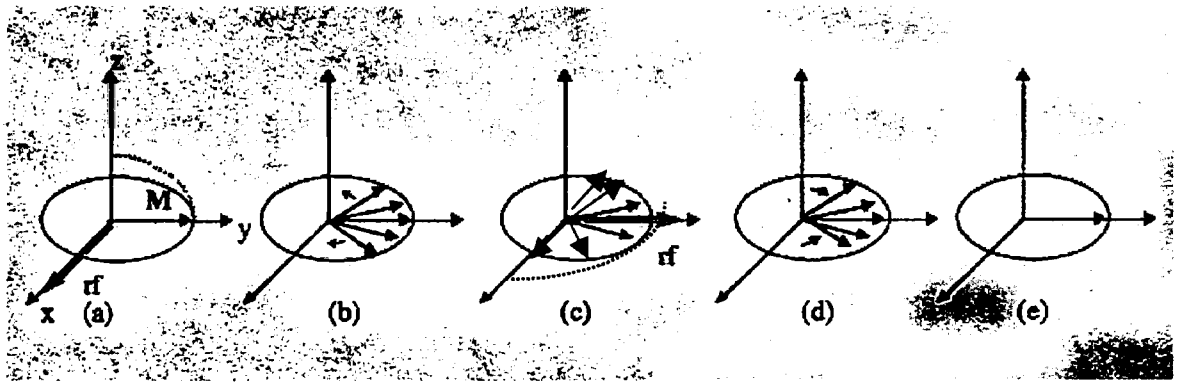

Figure 2.1 Spin echo pulse sequence: (a) a 90° rf pulse is applied and (b) shows the dephasing beginning. In (c) (at maximum dephasing) a 180° pulse is applied and (d) shows rephasing. In (e) the magnetization has completely rephased, producing a large induction signal or spin echo.

2.1.2 48 Echo CPMG Experiment

Traditionally, the spin echo experiment has a single 180° pulse after the first 90° and the experiment must be repeated many times with many different tau values, so that a decay curve may be plotted and T_2 times extracted. A unique modification of this experiment is to have a train of 180° pulses after the 90° pulse and take data readings after each 180° pulse. This is called a Carr-Purcell-Meiboom-Gill (CPMG) echo train [7,8]. The pulse sequence used in this work was a 48 echo CPMG, where 48 180° pulses follow a single 90°. In this experiment, the first 32 180° pulses were 10ms apart, and the last 16 were 50ms apart. This 48 echo CPMG experiment is a modification of a 32 echo experiment in which all 180° pulses are 10ms apart. The 48 180° pulses were rectangular composite pulses flanked by slice-select crusher gradient pulses of alternating sign with descending amplitude for elimination of stimulated echoes and signal from outside the selected slice [9]. The pulse sequence diagram for the first portion of this experiment is shown in Figure 2.

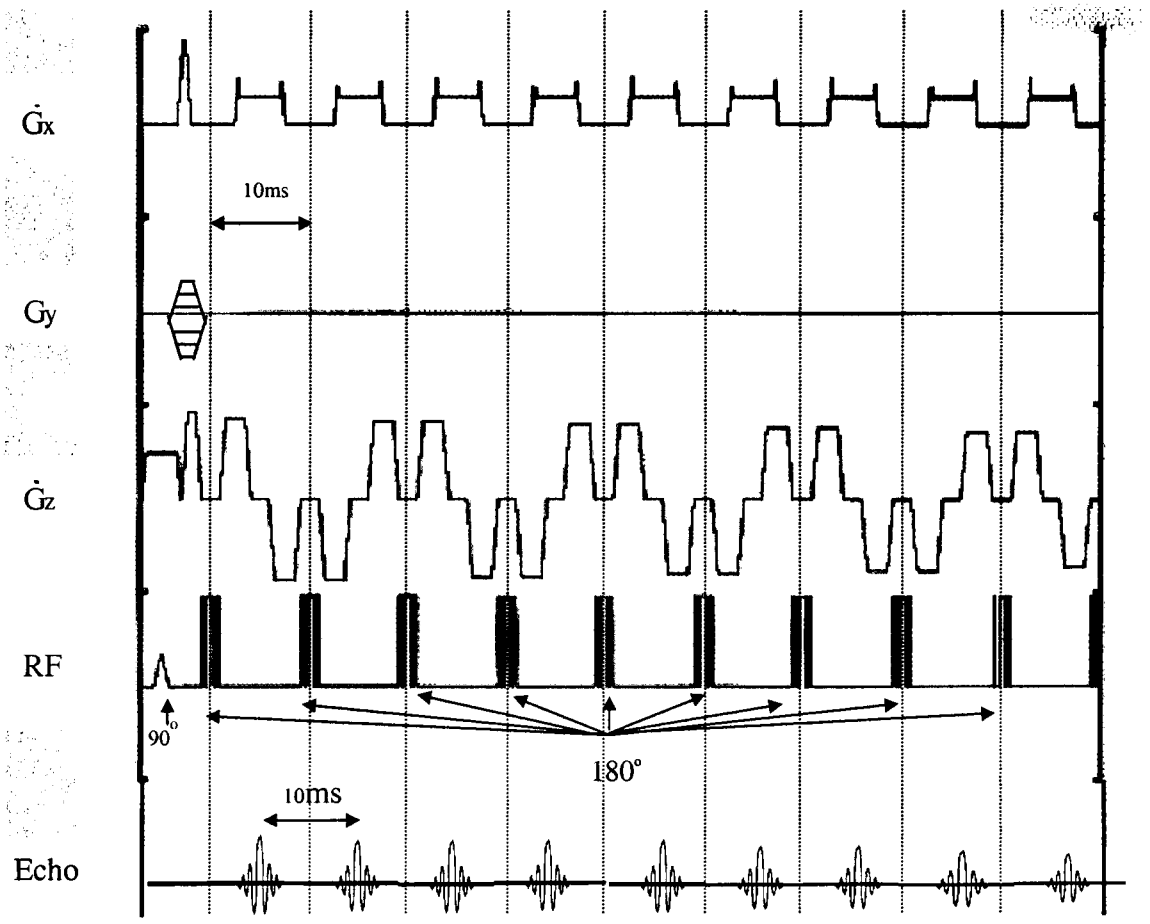

Figure 2.2 A pulse sequence diagram for a portion of our 48 echo sequence

2.2 Data Analysis

After a particular pulse sequence has been applied and data has been collected, analysis must be done to the data to extract the desired information. The CPMG experiment described in the previous section provides T_2 information. The first step towards determining the T_2 relaxation times is creating a plot of signal amplitude versus echo time as in figure 2.3

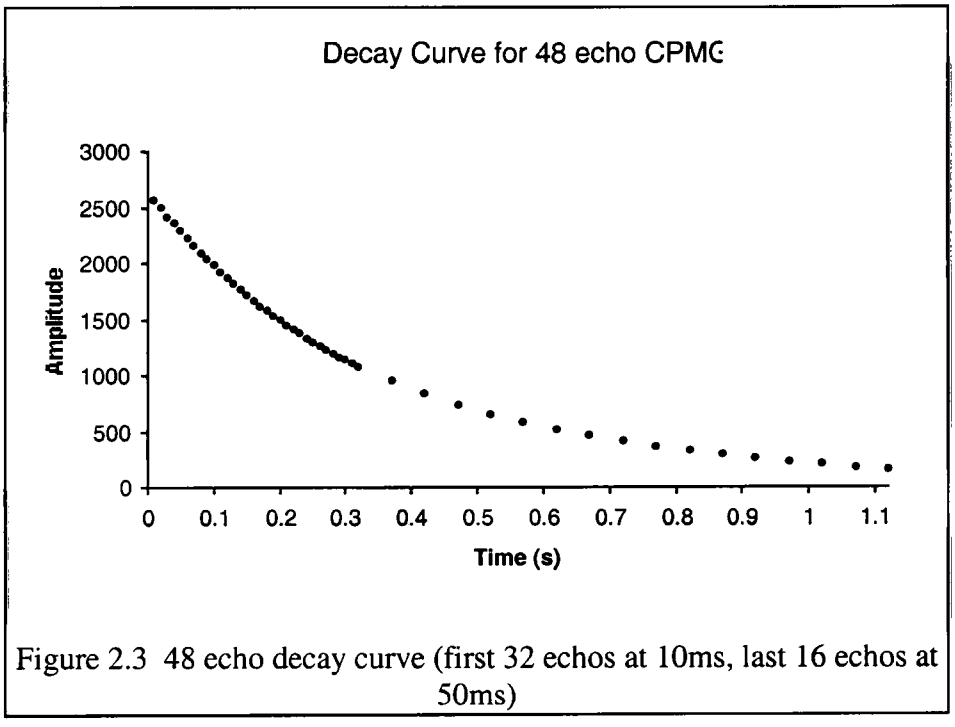

Figure 2.3 48 echo decay curve (first 32 echos at 10ms, last 16 echos at 50ms)

This data is then fit to a multi-exponential curve of the form

$$\text{Amp}\ (\text{TE}\ ) = \sum_{i=1}^{N} A_i e^{\frac{-\text{TE}}{T_{2i}}}$$

using a modified non-negative least squares fitting routine (NNLS) [10,11] One hundred and sixty T_2 times ranging from 1ms to 10s are input and there are no apriori assumptions

about the number of exponential components in the decay curve. NNLS analysis gives a discrete T_2 distribution made up of delta functions as the lowest chi squared fit to a decay curve. The true T_2 distribution from brain is more likely composed of a continuous distribution of relaxation times, so to accommodate for this, chi squared was allowed to increase from 1-2% by minimizing solution roughness, as well as chi squared. [12] A typical T_2 distribution is shown in figure 2.4 .

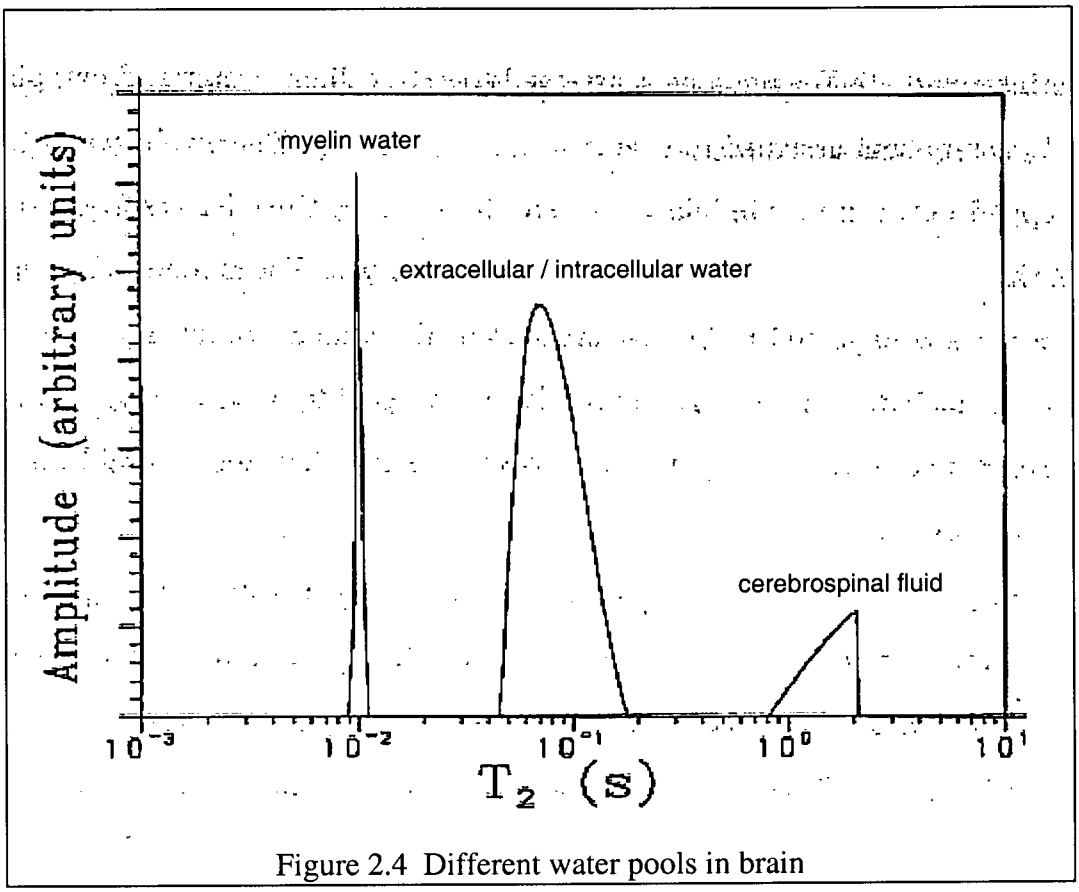

Figure 2.4 Different water pools in brain

The T_2 relaxation times are dtermined by the environment that the hydrogen is found in. The hydrogen signal found in brain by MRI is primarily in the form of water and can be separted into three environments or different pools based on relaxation time. The first

pool is Cerebrospinal fluid (CSF), which is a liquid that surrounds the brain and prevents it from hitting the skull. CSF has the longest relaxation time of around 1s. The second pool makes up Intra and extracellular water which is trapped within and surrounding the cells. Intra and extracellular water has an average relaxation time of about 80ms. The third environment of water is myelin water which is trapped between the myelin bilayers that surround the axon. Myelin water has a relaxation time of about 10-40ms. The amount of myelin water present is hypothesized to directly correlate to the amount of myelin. [7]

One method of looking at the amount of myelin present is to determine the fraction of myelin water in different white and grey matter structures in the brain. This is done by drawing a region of interest (ROI) in a certain area on an image and calculating the fraction of myelin water in that area. The area underneath of each T_2 peak corresponds to the number of protons which contribute to that signal. The fraction of myelin water is defined as:

$$fr = \frac{Area_{myelin.water.peak}}{Area_{all.peaks}} \qquad (1.8)$$

Figure 2.5 shows different white and grey matter structures and Figure 2.6. shows myelin fraction for different structures.

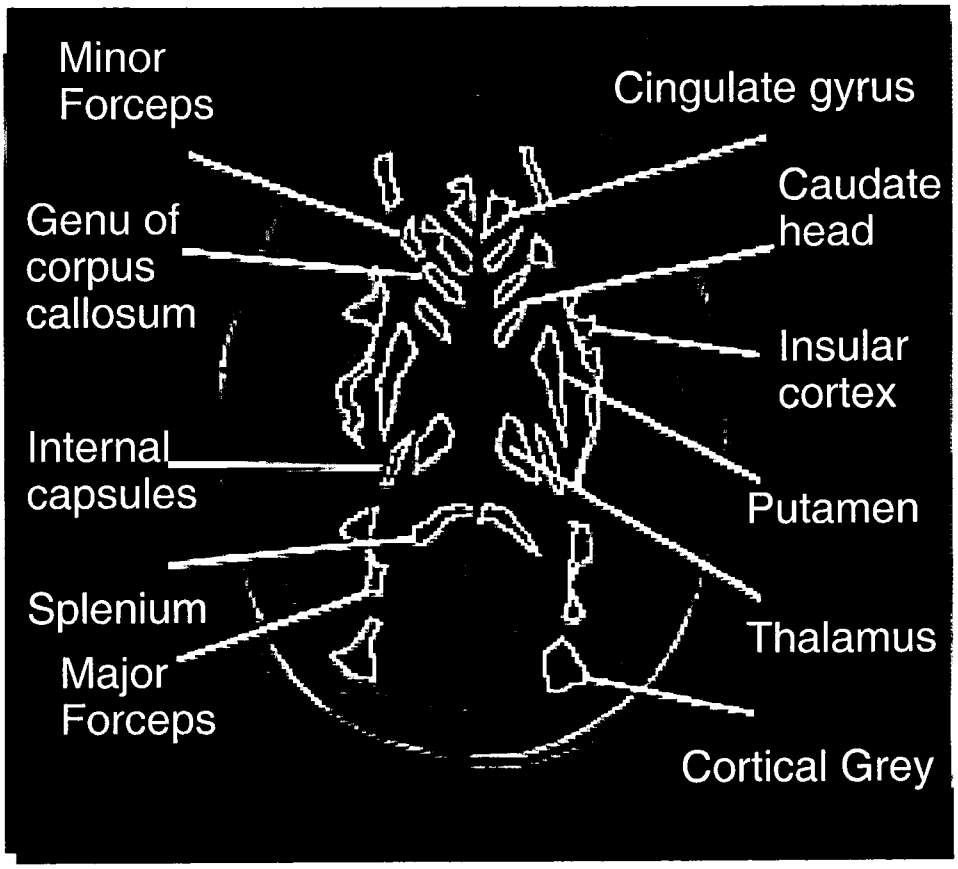

Figure 2.5 White and grey matter structures in brain

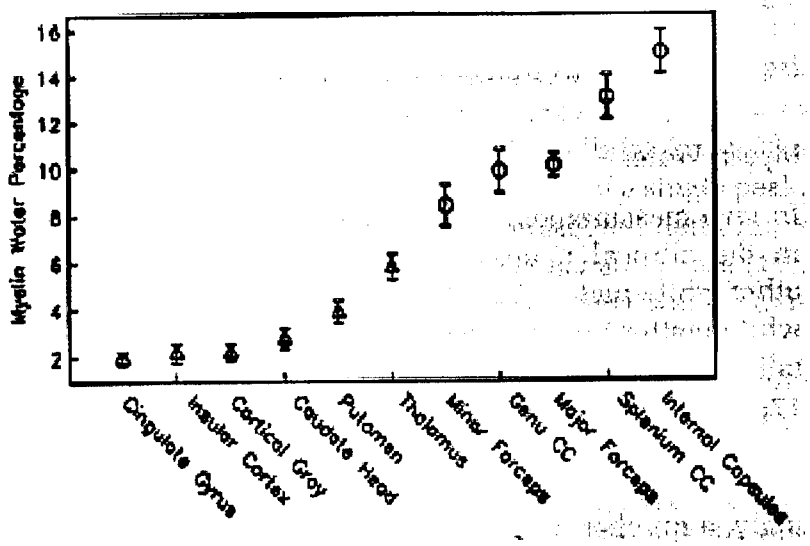

Figure 2.6 Fraction myelin water versus structure

Another method of examining the amount of myelin water in brain is to determine the fraction myelin water at each pixel in the image and display that as a resulting image. Figure 2.7 shows such a resulting myelin map. Brigher intensity means more myelin.

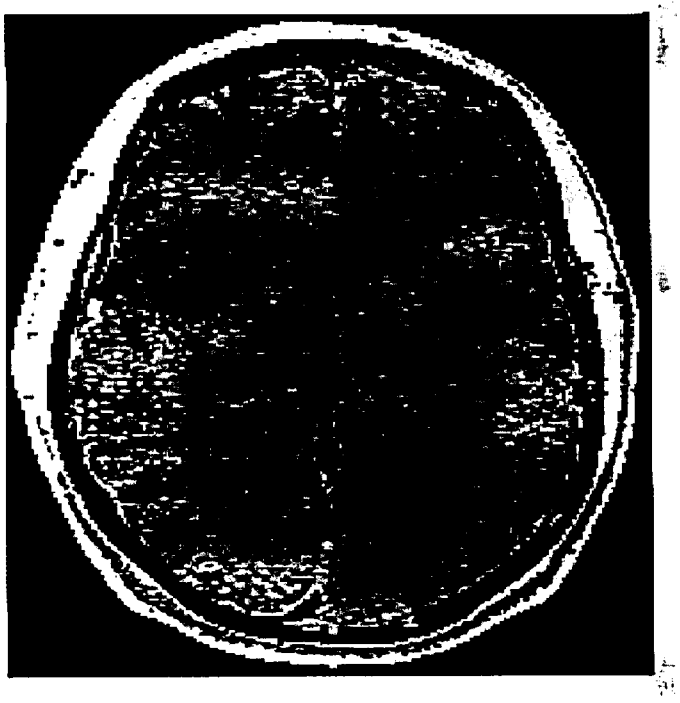

Figure 2.7 Typical myelin map

Both investigating specific regions of interest and creating whole brain myelin maps are valuable tools for studying myelin.

2.3 Motivation

In order to better study the intermediate T_2 component(s), especially in lesions, our 32 echo T_2 measurement sequence (TE10-TE320) was lengthened by 16 echoes with echo spacing 50ms, as described in section 2.1. To maintain the same T_1 weighting, the TR was increased from 3s to 3.88s. Scan time is defined as

$$\text{Scan.Time} = TR * N_{averages} * N_{phase\_encodes}$$

where the number of averages = 4 and the number of phase encodes is 128. By changing the TR from 3s to 3.88s, the scan time increases to 33 minutes. To investigate multiple sclerosis using T_2 relaxation, the scan time must be clinically feasible, so the goal of this thesis was to shorten the acquisition time for T_2 measurement by collecting higher order k-space lines with shorter TR. [13,14], with out sacrificing image quality.

Chapter 3

Variable TR Simulations

3.1 Summary

Variable TR MRI images were simulated using five spin-echo images collected at different TR times. Different lines of k-space were extracted from each image and recombined to make a single image using several computer programs. The resulting images were qualitatively analyzed.

3.2 Introduction

The time available on the MRI scanner is both limited and expensive, so often before collecting actual data, computer simulations are performed to investigate expected results. By simulating many different possible outcomes of the variable TR pulse sequence, we were given the opportunity to visually inspect the images. This gave a clearer idea of what the variable TR images would look like and allowed us to wisely choose which parameters to use in the future during actual data collection.

3.3 Methods

Five spin-echo weighted images were collected from one volunteer for the same slice at five different TR times. The five different TR times were: 1000ms, 1400ms, 1880ms, 2260ms and 2680ms. Constant parameters for all five scans were TE = 10ms, FOV = 22cm, bandwidth 32 kHz, matrix size 256 x 128 and NEX = 4. All experiments were done on a 1.5T General Electric Signa clinical MR Scanner. Figures 3.1 to 3.5 show the five T_1 weighted images.

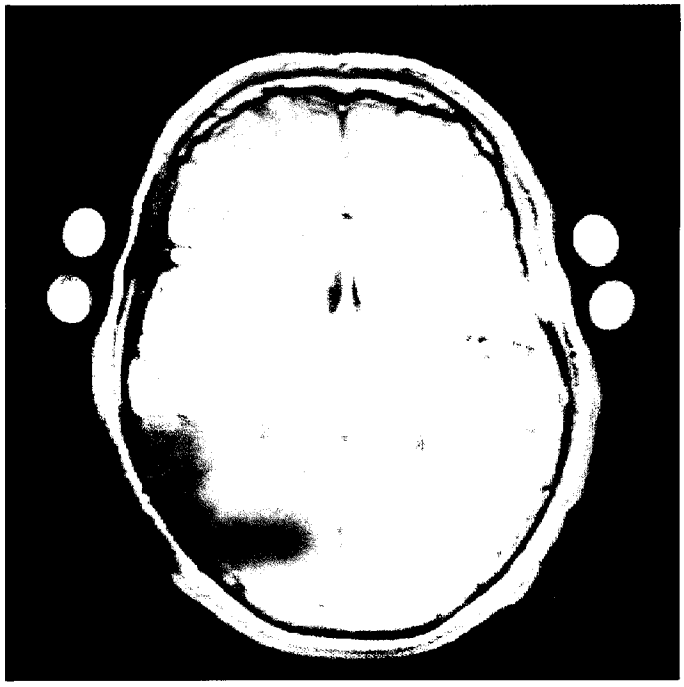

Figure 3.1 Spin-echo image with TR of 1000ms

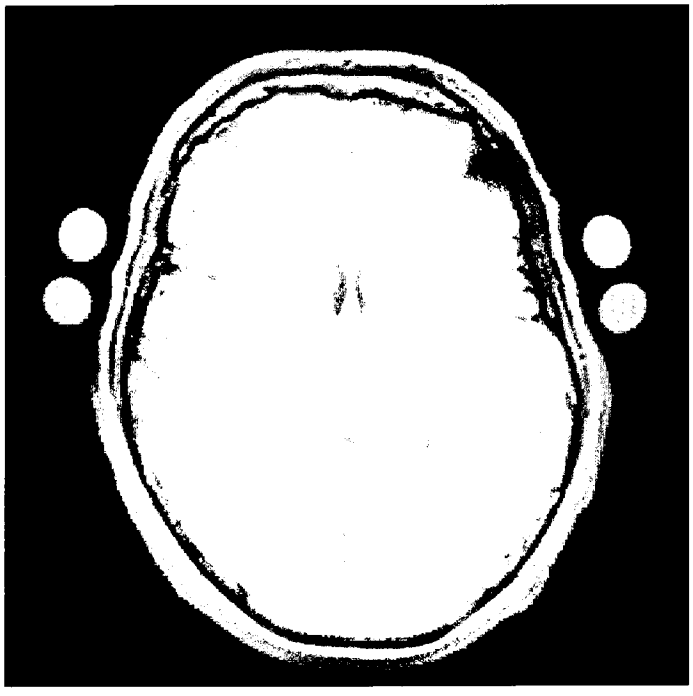

Figure 3.2 Spin-echo image with TR of 1400ms

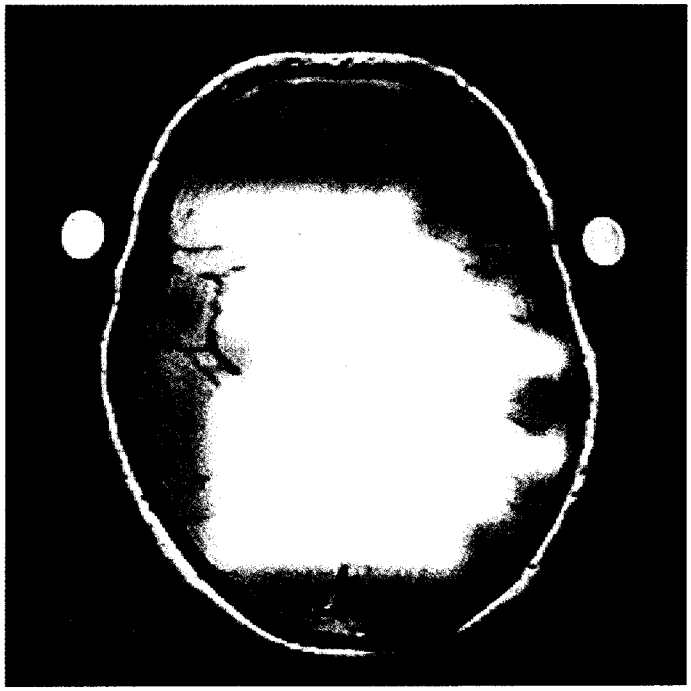

Figure 3.3 Spin-echo image with TR of 1880ms

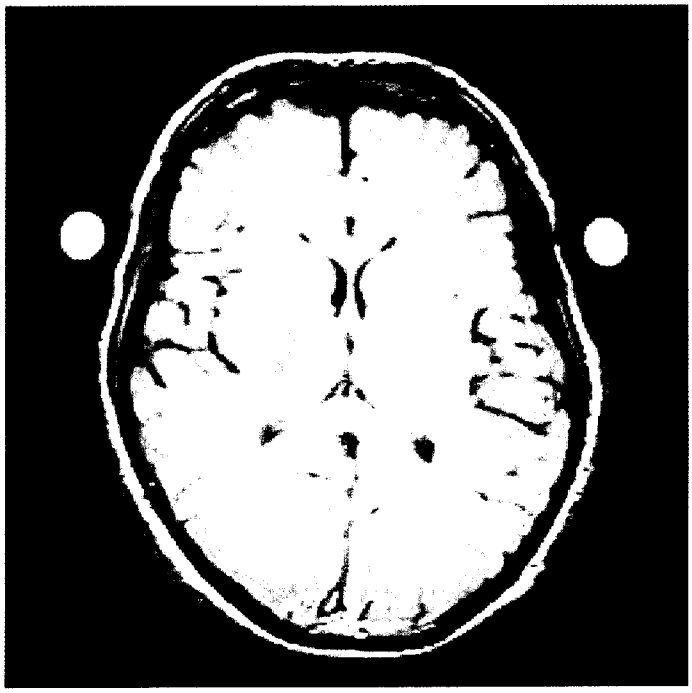

Figure 3.4 Spin-echo image with TR of 2260ms

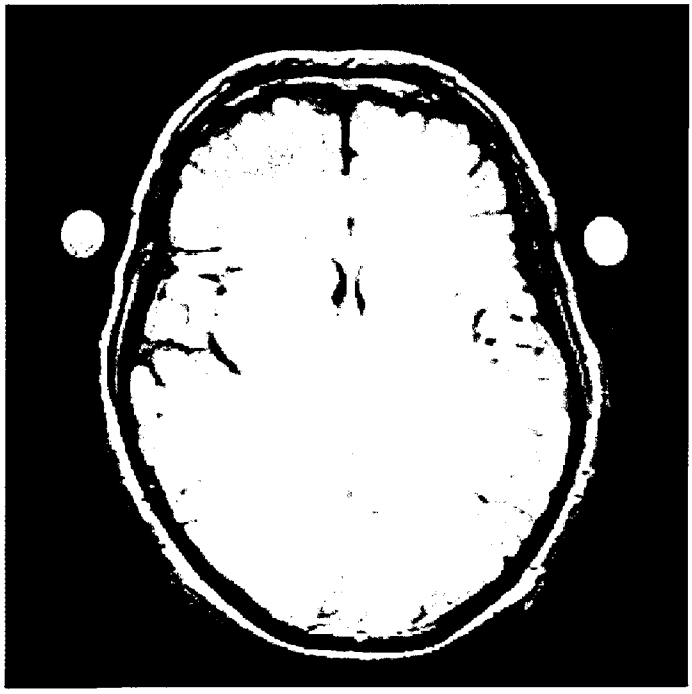

Figure 3.5 Spin-echo image with TR of 2680ms

The amount of signal seen in the five previous images increases as TR increases. As discussed in section 1.3.4, TR is the repetition time between collecting data for successive line of k-space. As this time increases, the amount of magnetization which has relaxed back to equilibrium increases and there is more longitudinal signal available to excite at the beginning of the next experiment.

3.4 Results

3.4.1 Various Combinations of TR

The raw or k-space data from these five images were used to create variable TR simulations. Specific lines were chosen from each image and combined into a single matrix. Figure 3.6a shows the k-space trajectory for n = 5. The first 5 lines were taken from the TR = 1000ms image. Then 1 line from TR = 1440ms, 1 line from 1880ms and 1 line from 2260ms. The middle 112 lines were taken from the image with TR = 2680ms.

A ramp down occurs with 1 line from the TR = 2260ms, 1 line from the TR = 1880ms and 1 line from TR = 1400ms. The last 5 lines are from TR of 1000ms. Figure 3.6b shows the Fourier transform of the data, the resulting image.

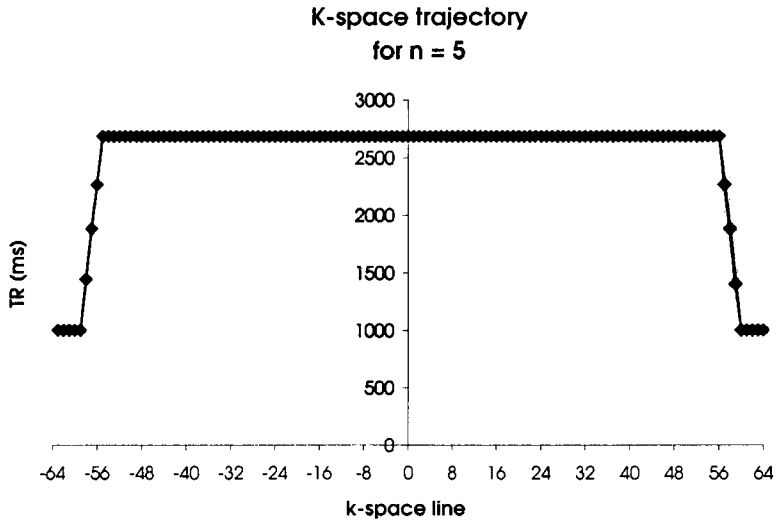

(a)

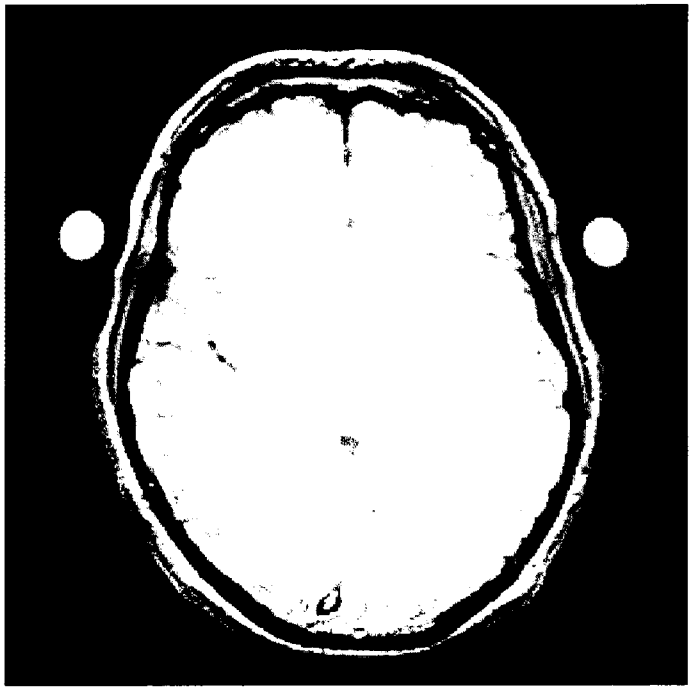

(b)

Figure 3.6 (a) k-space trajectory and (b) image for n=5 (31 minutes)

Figures 3.7 to 3.15 show similar k-space trajectories and images for n = 10, 15, 20, 25, 30, 35, 40, 45 and 50. Table 3.1 summarizes the time for each scan.

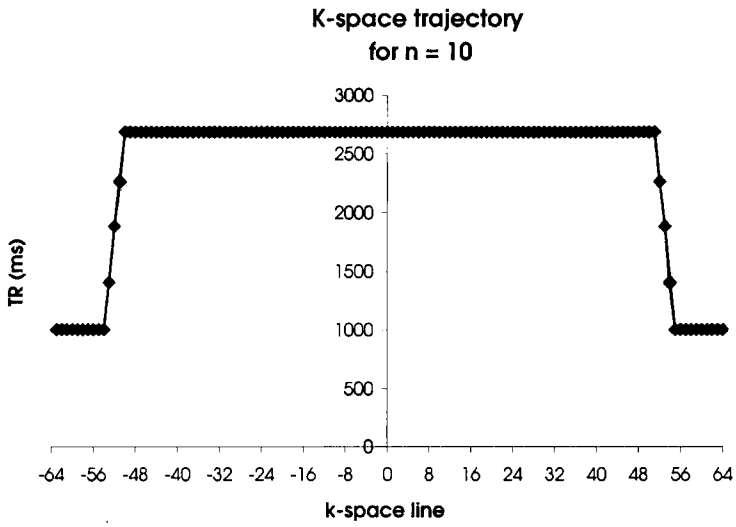

(a)

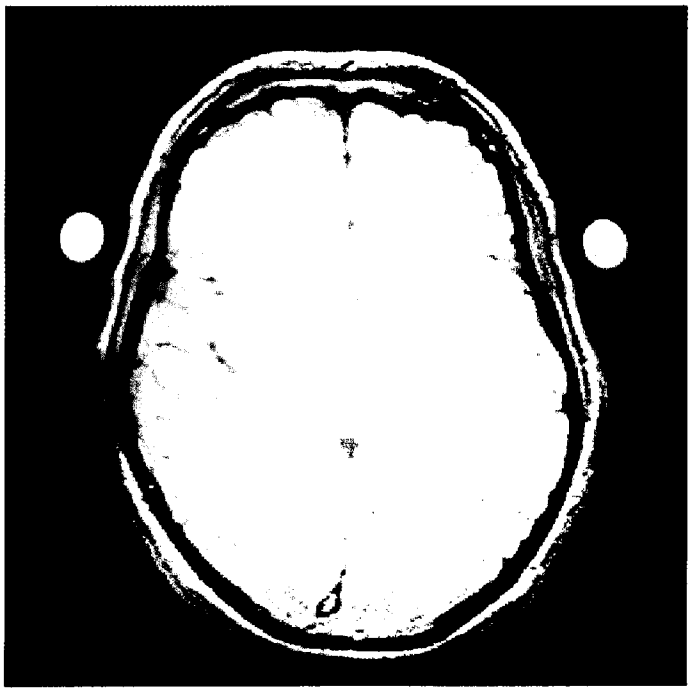

(b)

Figure 3.7 (a) k-space trajectory and (b) image for n=10 (30 minutes)

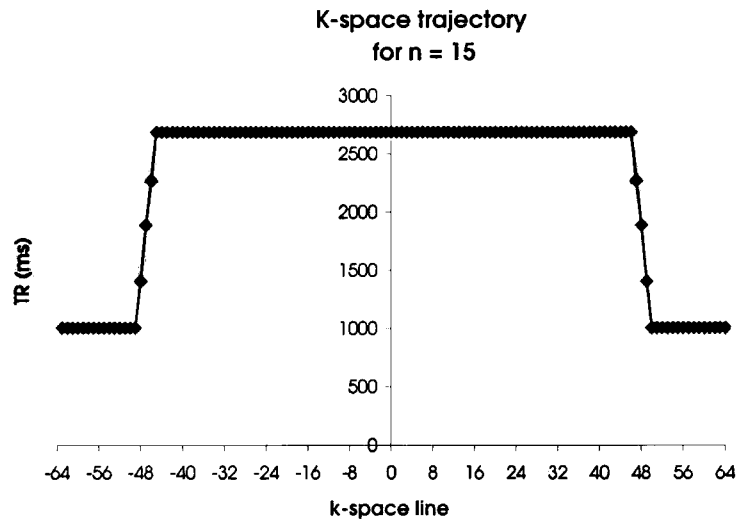

(a)

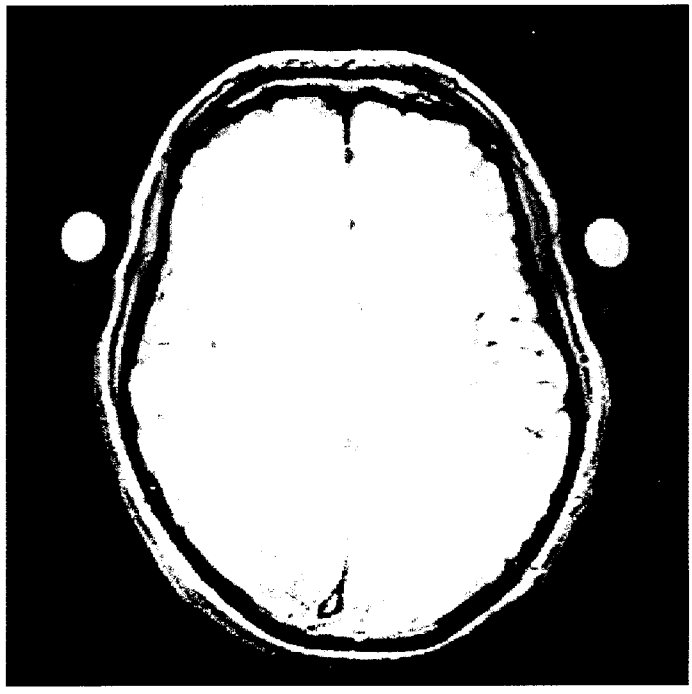

(b)

Figure 3.8 (a) k-space trajectory and (b) image for n=15 (29 minutes)

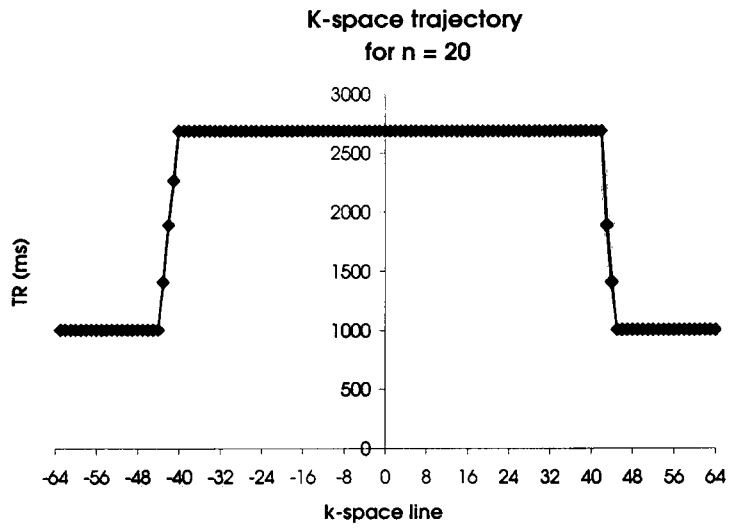

(a)

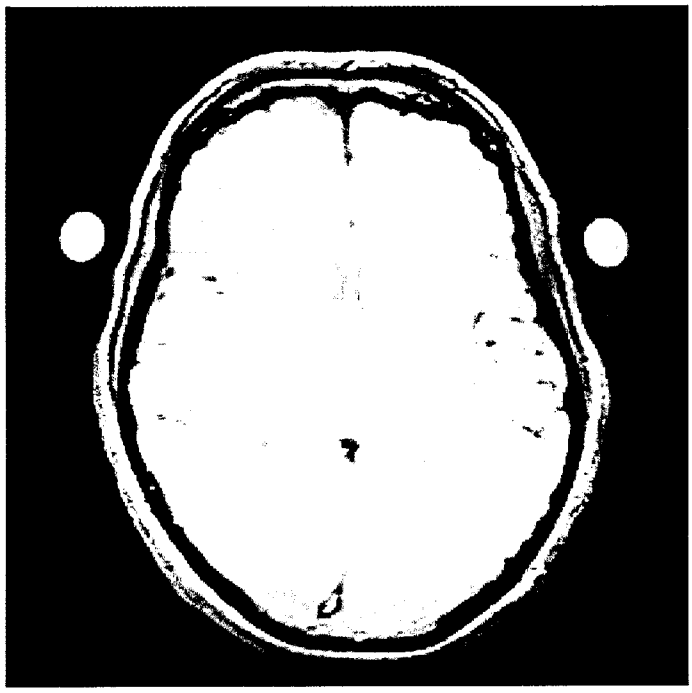

(b)

Figure 3.9 (a) k-space trajectory and (b) image for n=20 (28 minutes)

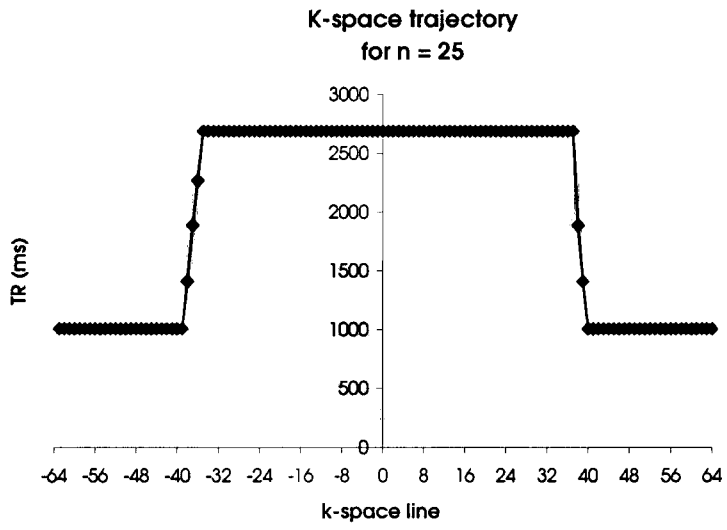

(a)

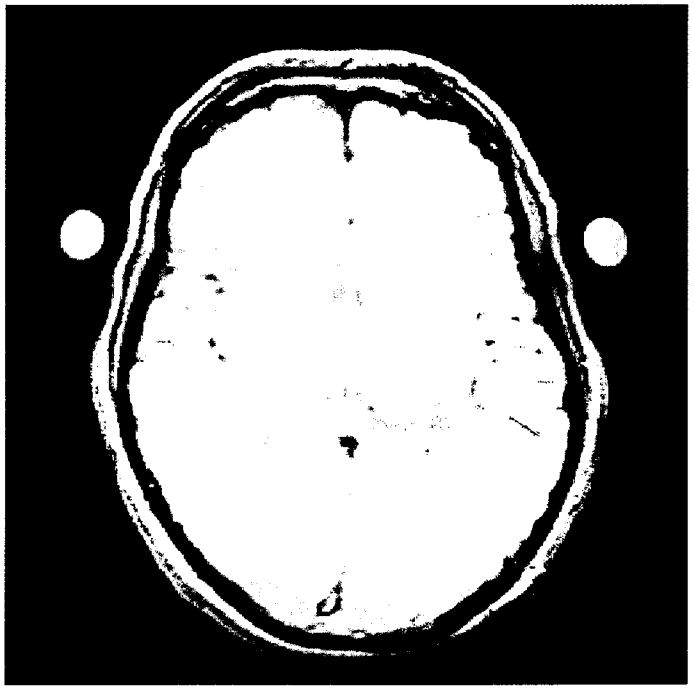

(b)

Figure 3.10 (a) k-space trajectory and (b) image for n=25 (26 minutes)

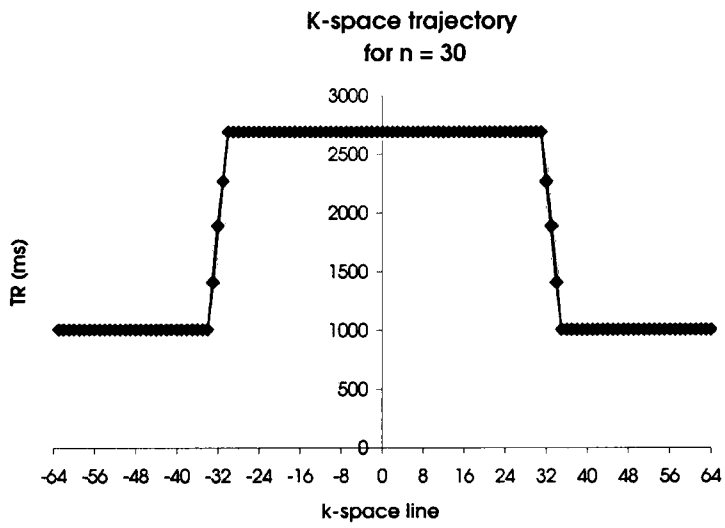

(a)

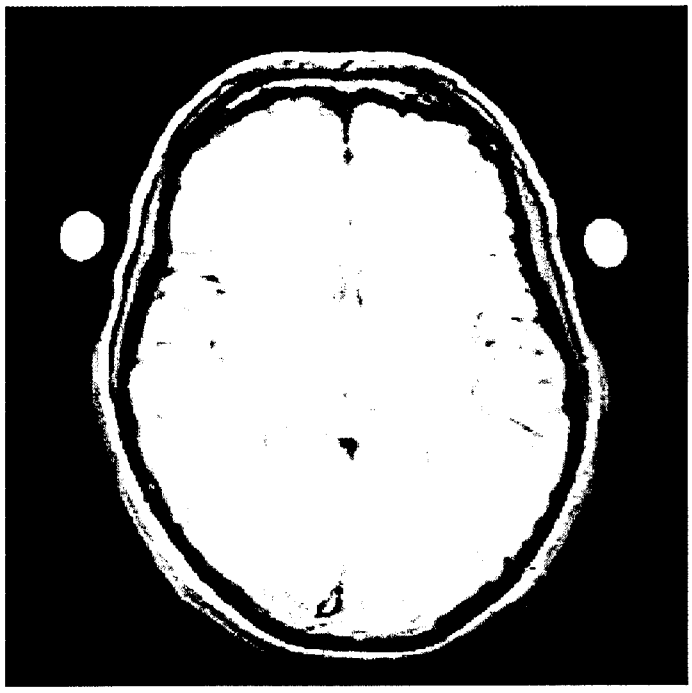

(b)

Figure 3.11 (a) k-space trajectory and (b) image for n=30 (25 minutes)

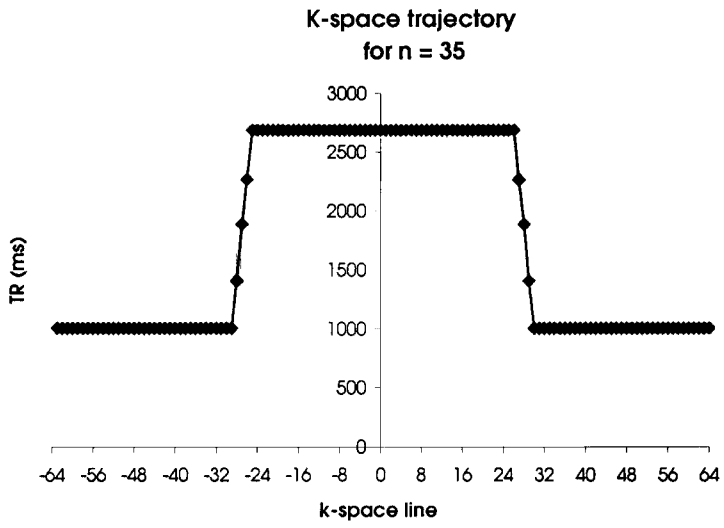

(a)

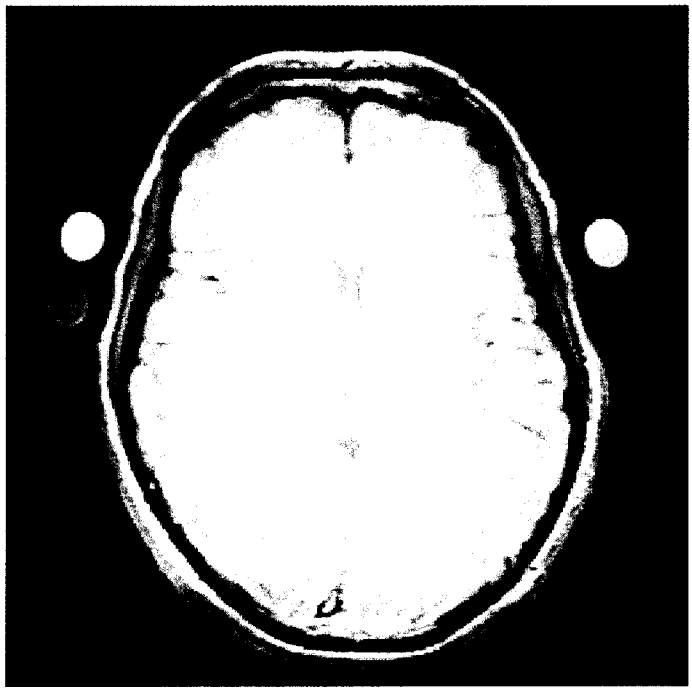

(b)

Figure 3.12 (a) k-space trajectory and (b) image for n=35 (24 minutes)

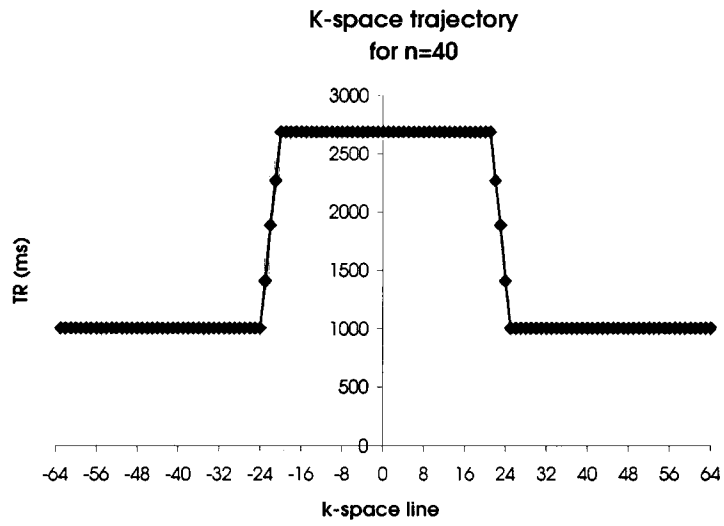

(a)

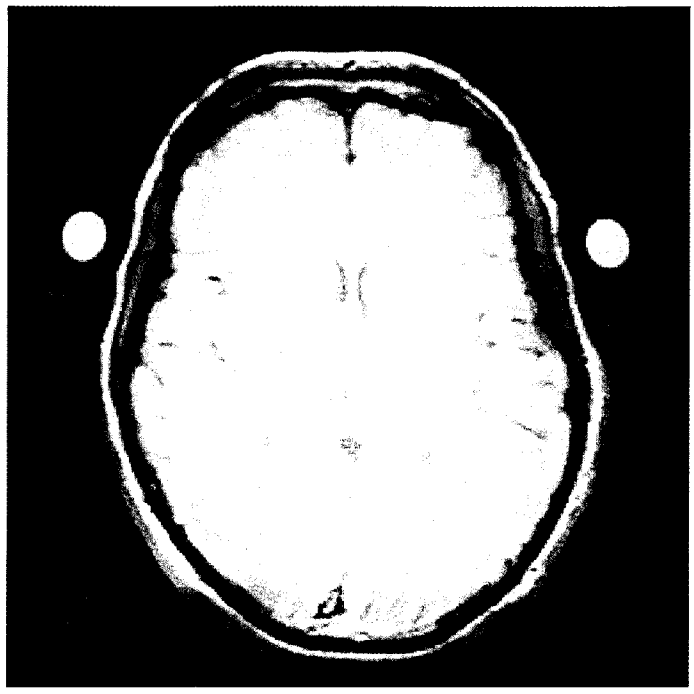

(b)

Figure 3.13 (a) k-space trajectory and (b) image for n=40 (23 minutes)

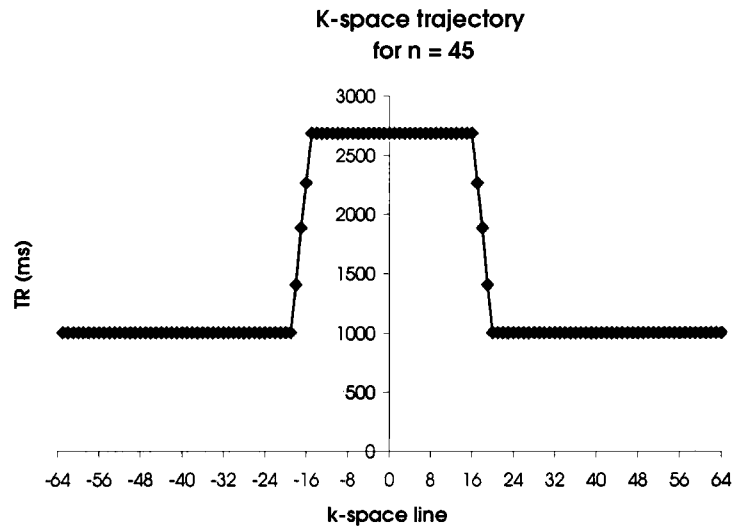

(a)

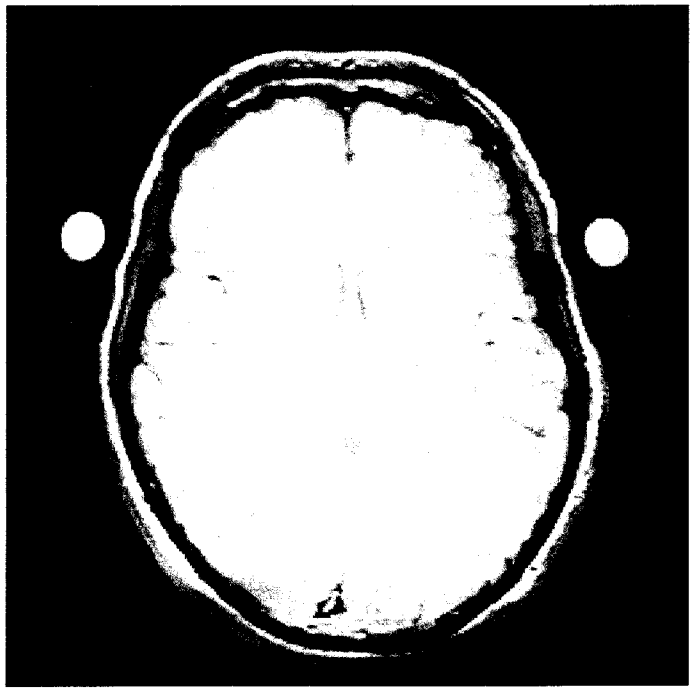

(b)

Figure 3.14 (a) k-space trajectory and (b) image for n=45 (22 minutes)

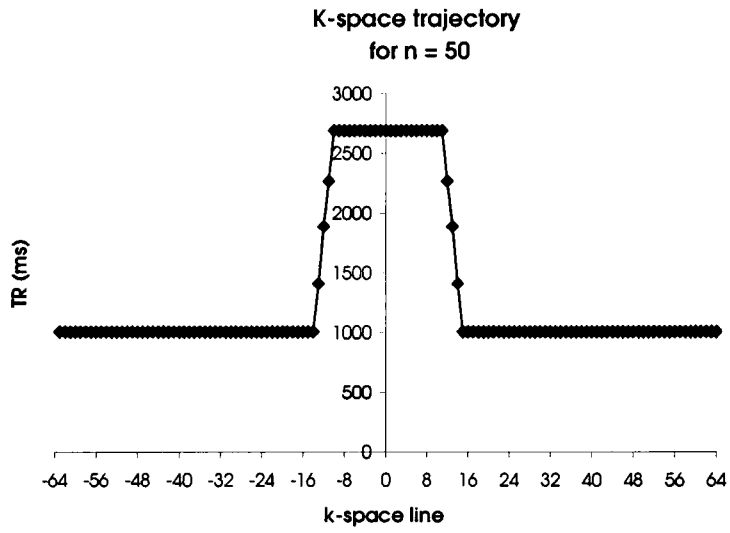

(a)

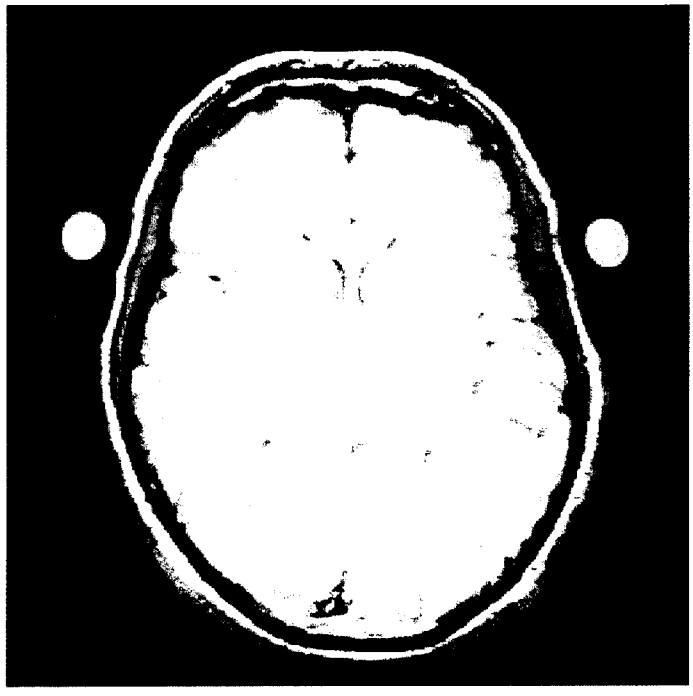

(b)

Figure 3.15 (a) k-space trajectory and (b) image for n=50 (21 minutes)

As n increases, the bluriness in the image also increases. As discussed in section 1.3.5, the higher order regions of k-space correspond to fine detail, so if this data is collected at a shorter TR time there is less longitudinal signal available for each excitation. Therefore,

the more lines that are collected at shorter TR, the blurrier the image becomes. Table 3.1 summarizes the amount of time each of the previous images would take to collect using the 48 echo variable TR sequence.

Table 3.1 Summary of Scan time as a function of n

n	Scan Time (minutes)
5	31.0
10	29.9
15	28.7
20	27.6
25	26.5
30	25.3
35	24.2
40	23.1
45	22.0
50	20.9

3.4.2 Difference Images of Simulations

To investigate the amount of resolution (sharpness) lost by increasing n, each simulated image was subtracted from the TR = 2680ms image (figure 3.5). Figures 3.16 to 3.18 show these difference images.

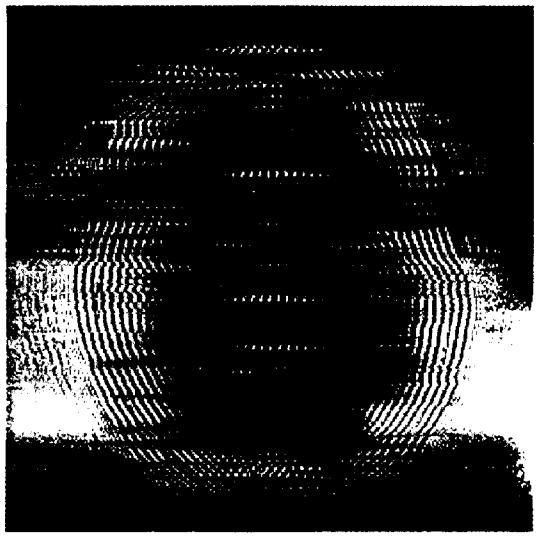

n=5

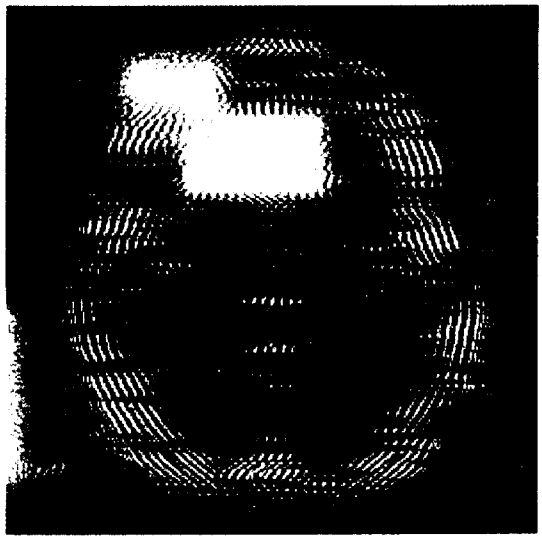

n=10

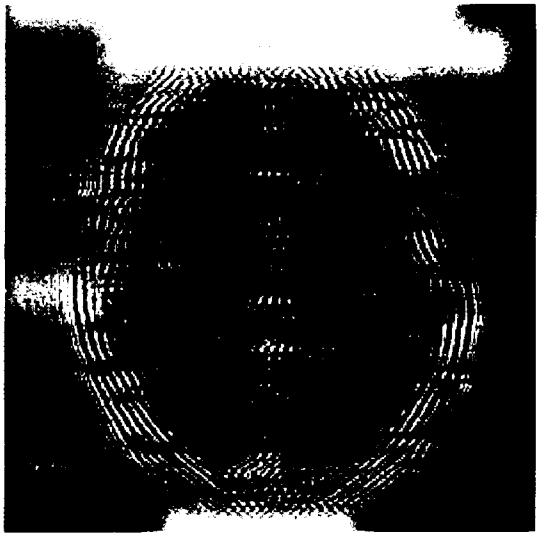

n=15

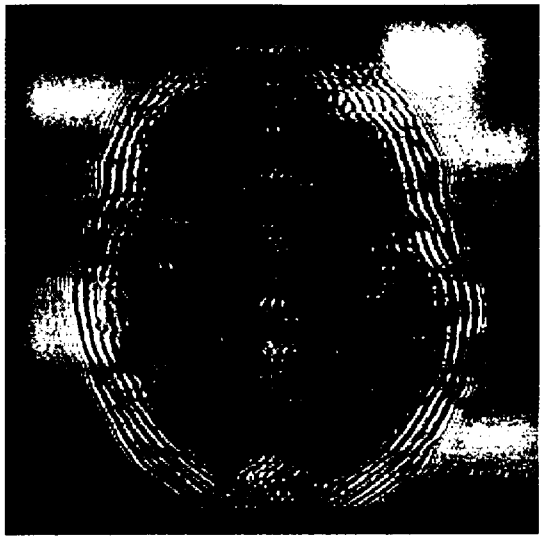

n=20

Figure 3.16 Difference images for n = 5, 10, 15 and 20

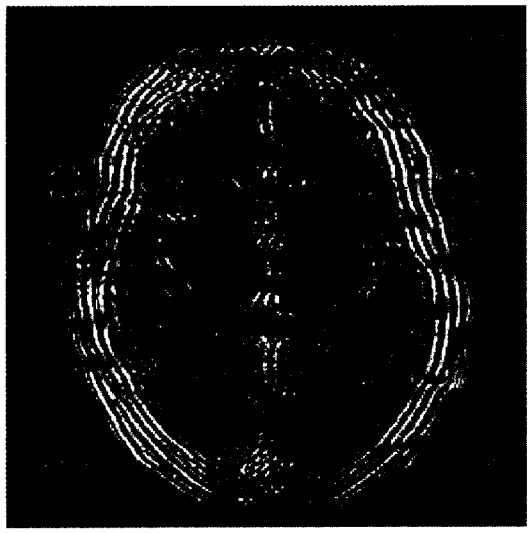

n=25

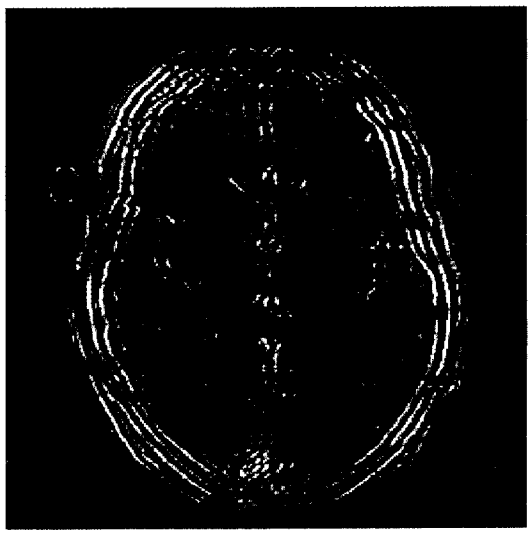

n=30

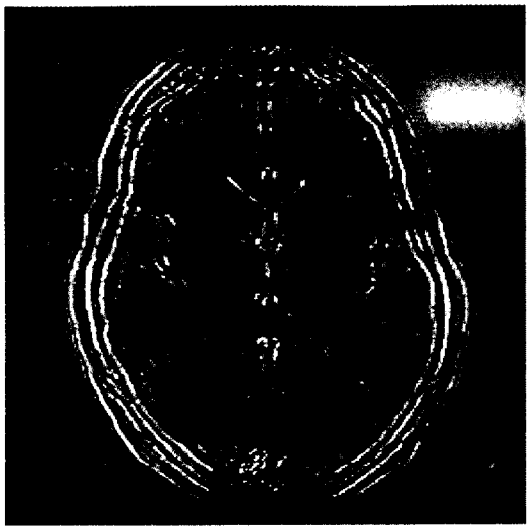

n=35

n=40

Figure 3.17 Difference images for n = 25, 30, 35 and 40

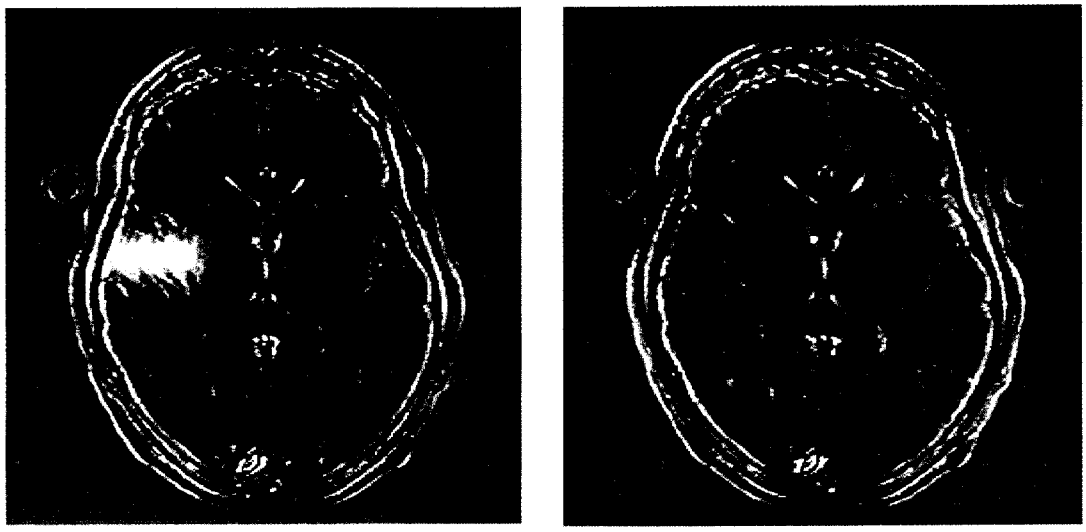

n=45 n=50

Figure 3.18 Difference images for n = 45 and 50

In the difference images for larger n, the differences become more noticable. Figure 3.17, n=35 shows some white matter structures beginning to appear, indicating they are not present in the simulated image. By figure 3.18, n=50 many structures are more visible.

3.5 Discussion

From the five spin-echo images, 10 variable TR simulations were created. Since the higher order k-space lines contribute to the sharpness or resolution of the final image, when a greater number of these lines were simulated to be collected at a shorter TR, the bluriness of the image increased. Investigating the difference of each simulated image with the spin-echo image with the longest TR, showed that as n increased, the amount of detail lost also increased.

3.6 Conclusion

By creating simulated variable TR images, we were able to qualitatively investigate the resulting bluriness of the images. Visual assessment of the created images and the difference images allowed us to determine what degree of resolution deterioration would still allow us to differentiate between important structures. It was decided that the simulation for n = 30 had the optimal decrease in scan time, without too great a compromise in image quality.

Chapter 4

48 Echo Variable TR on Phantoms

4.1 Summary

Nine phantoms were made with different combinations of T_1 and T_2 relaxation times. These phantoms were scanned using the 48 echo variable TR pulse sequence, as well as a T_1 saturation recovery. The relaxation times are summarized and the decay curves are shown. The dependence on n of density, geometric mean T_2 and chi squared are shown.

4.2 Introduction

Before performing MRI experiments on humans, it is typical to run the pulse sequences on a phantom. A phantom is a sample which takes the place of a live subject in the scanner and has known T_1 and T_2 relaxation times. By scanning a phantom, one can determine how well a new pulse sequence works by seeing if one obtains a good image. The expected relaxation times, density, and a reasonable chi squared can also be quantitatively examined.

4.3 Materials and Methods

4.3.1 Phantom Preperation

Nine different phantoms were made with different combinations of T_1 and T_2 relaxation times. The phantoms were made using nickel chloride and 1%, 2% and 4% agarose gel. The solutions were poured into 20cm long, 2 cm wide pyrex tubes and flame sealed under vacuum.

4.3.2 48 Echo Variable TR Pulse Sequence

In order to try and experimentally reproduce the results obtained in from the simulations in chapter 3, different lines of k-space needed to be collected at varying TR times. The traditional 48 echo experiment with a constant TR is described in section 2.1.2. This pulse sequence was modified such that certain lines of data could be collected at different TR times. Figure 4.1 shows a plot of TR as a function of k-space with scanner input parameters labeled.

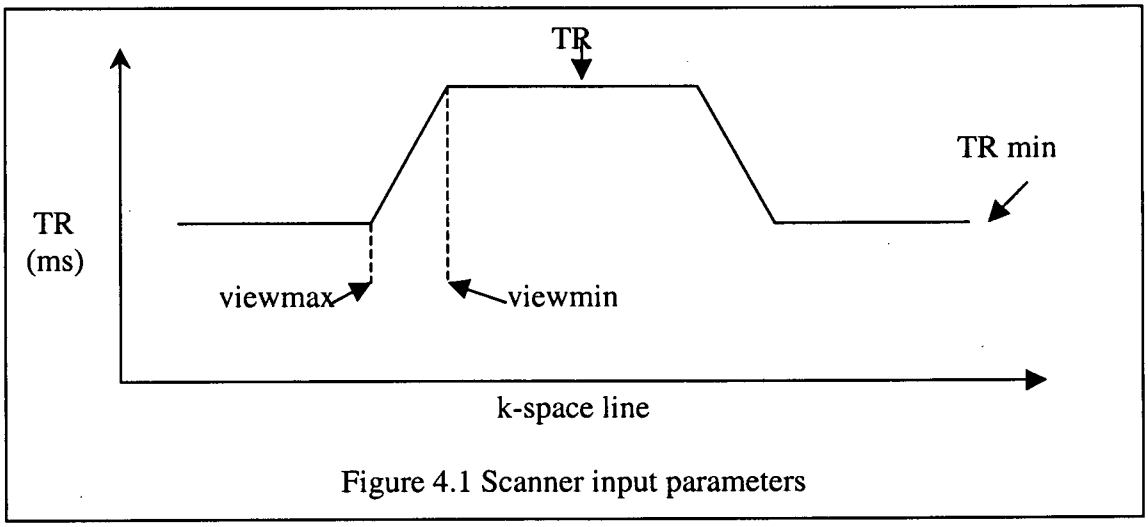

Figure 4.1 Scanner input parameters

Input parameters into the variable TR experiment were TR, TRmin, viewmin and viewmax. For example, for n = 30 where the first and last 30 lines of k-space are to be collected at a shorter TR, TR = 3800ms, Trmin = 2120ms, viewmax = 34 and viewmin = 30.

4.4 Results

4.4.1 T_1 and T_2 Relaxation times

The phantoms were first scanned using the 48 echo CPMG experiment outlined in section 2.1.2, with a TR of 3800ms for all views and 2 averages (NEX) to determine the

T_2. A saturation recovery experiment was used to find the T_1 relaxation times. Table 4.1 shows the different relaxation times for the nine phantoms.

Table 4.1 Phantom T_1 and T_2 Relaxation Times

Phantom	T_1 (ms)	T_2 (ms)
1	330	83
2	580	28
3	606	101
4	1640	28
5	300	25
6	1570	356
7	1640	108
8	372	188
9	718	258

4.4.2 Decay Curves

In order to investigate the differences between the variable and non-variable TR 48 echo pulse sequence, the decay curves from the phantoms bottles collected at various values of n were compared to the constant TR results. Figures 4.2 to 4.10 show decay curves for each phantom for n = 0 to n = 64.

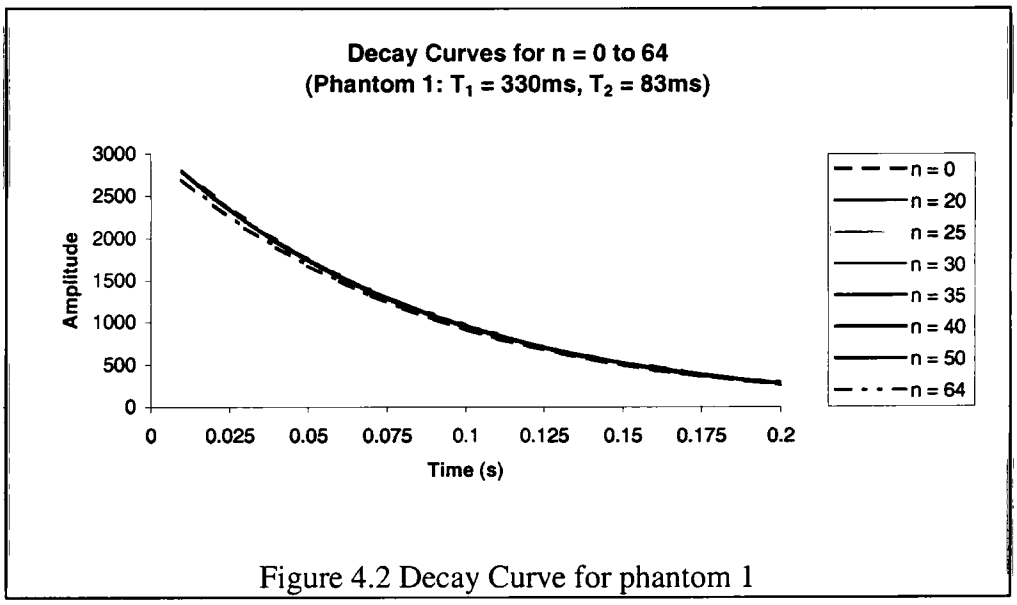

Figure 4.2 Decay Curve for phantom 1

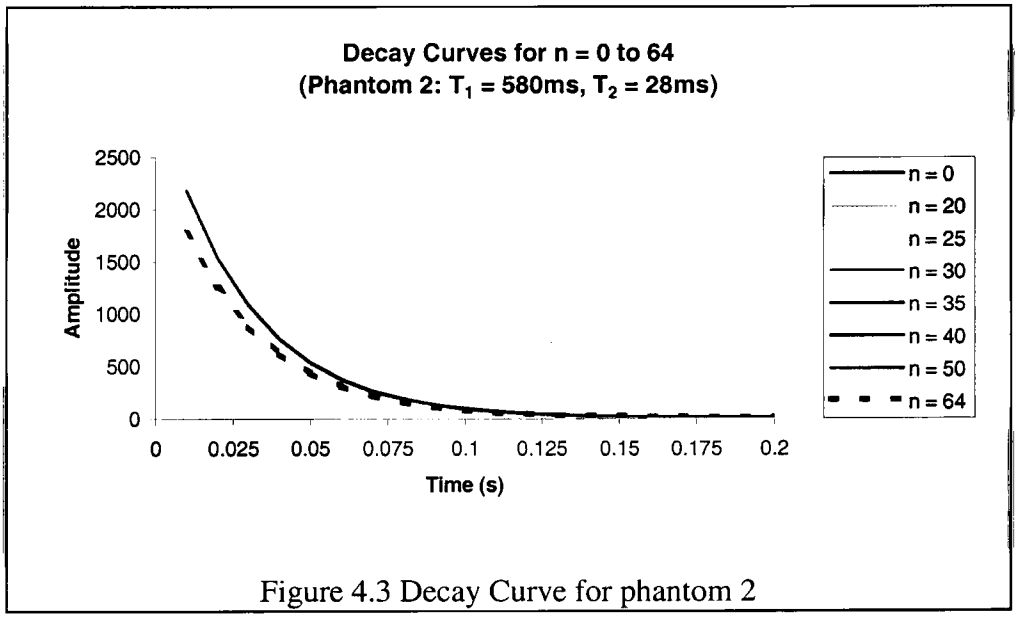

Figure 4.3 Decay Curve for phantom 2

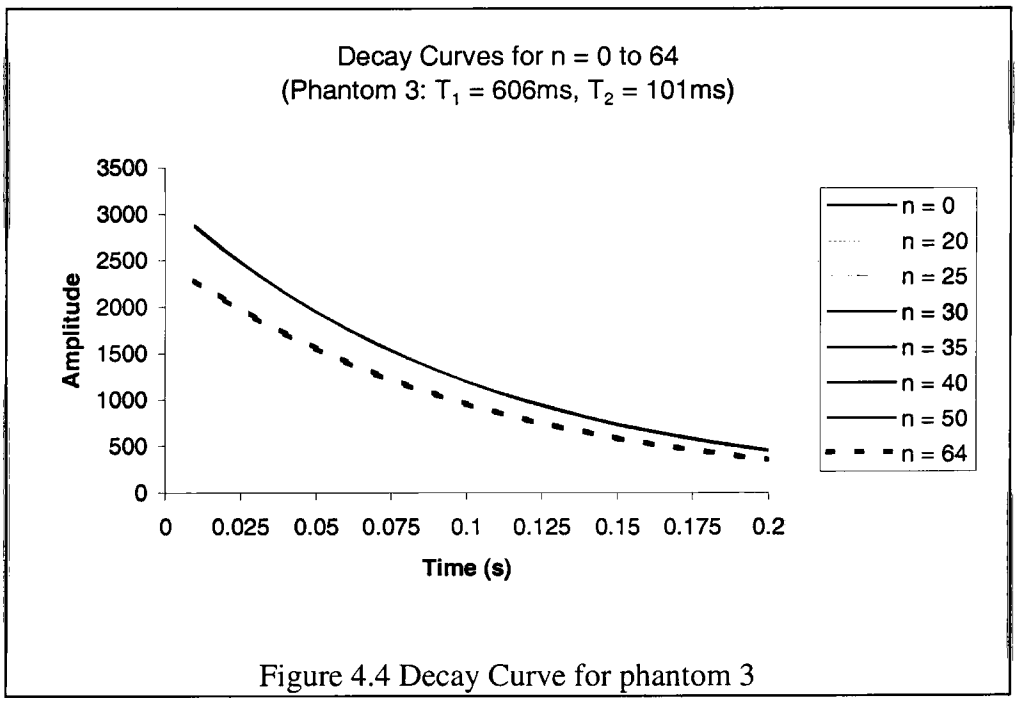

Figure 4.4 Decay Curve for phantom 3

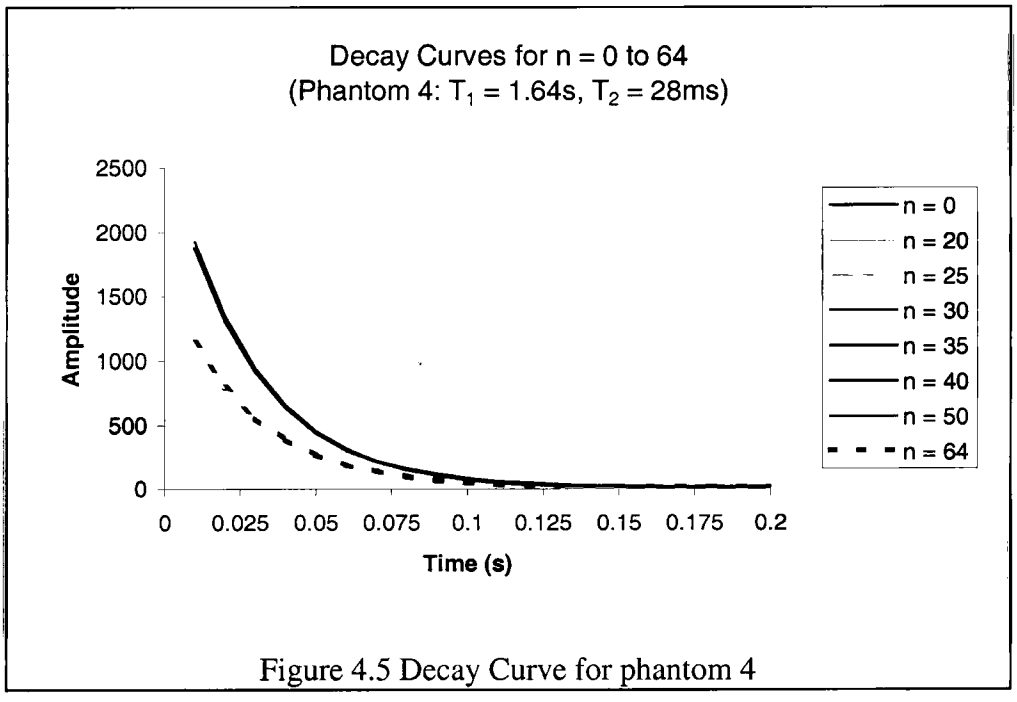

Figure 4.5 Decay Curve for phantom 4

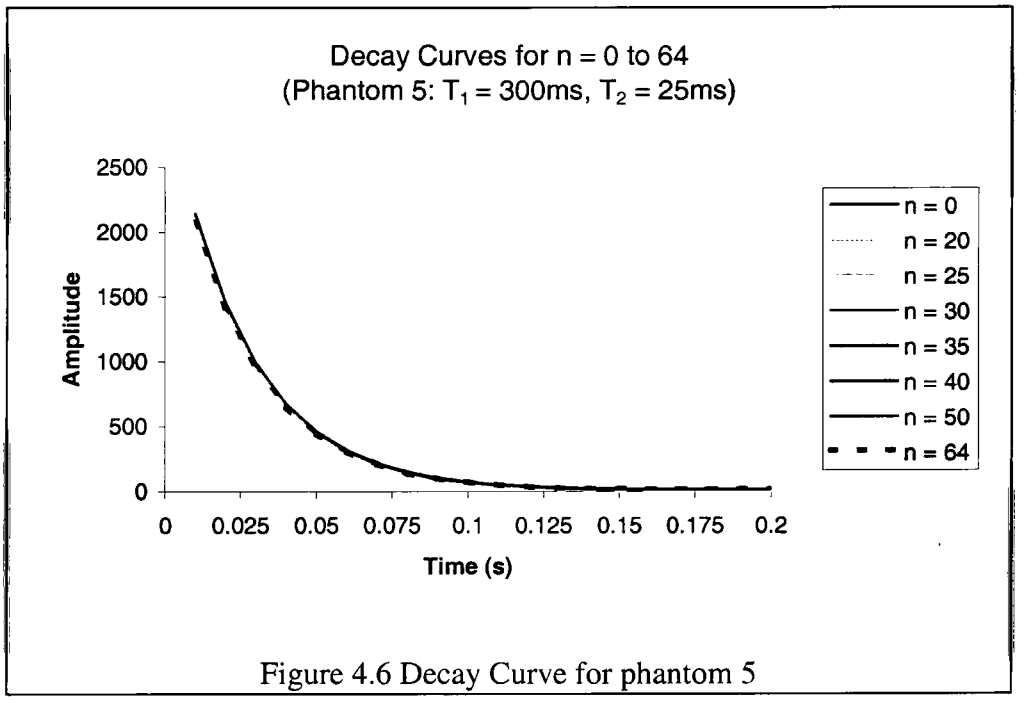

Figure 4.6 Decay Curve for phantom 5

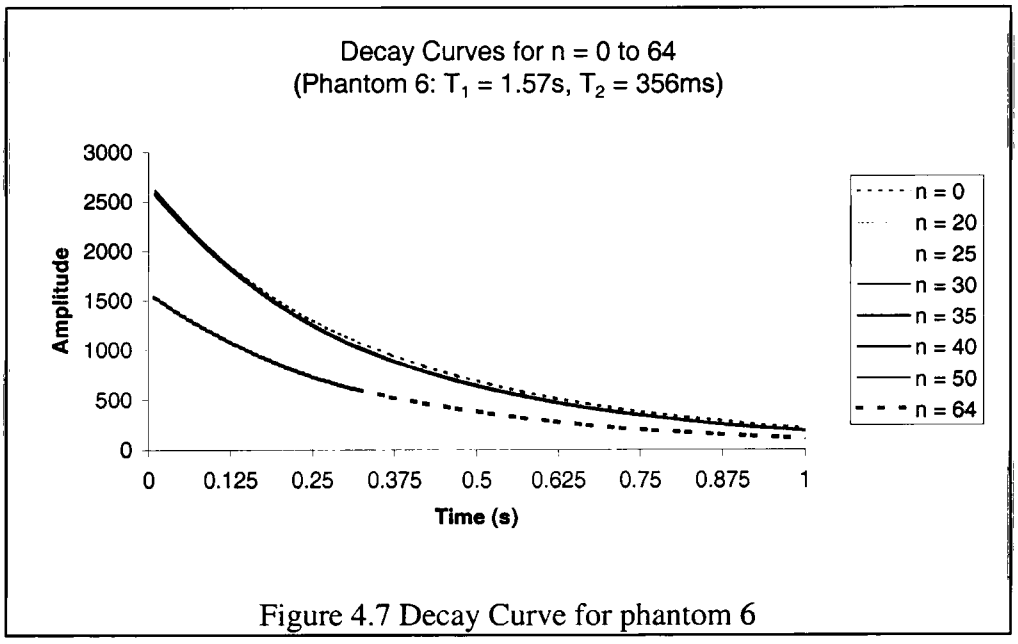

Figure 4.7 Decay Curve for phantom 6

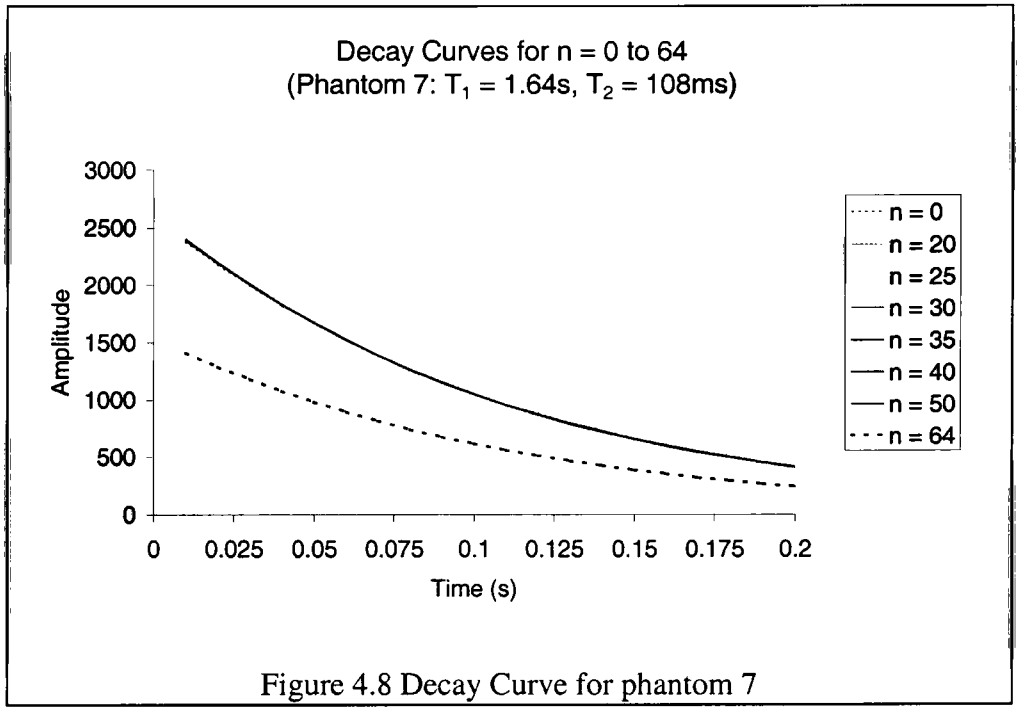

Figure 4.8 Decay Curve for phantom 7

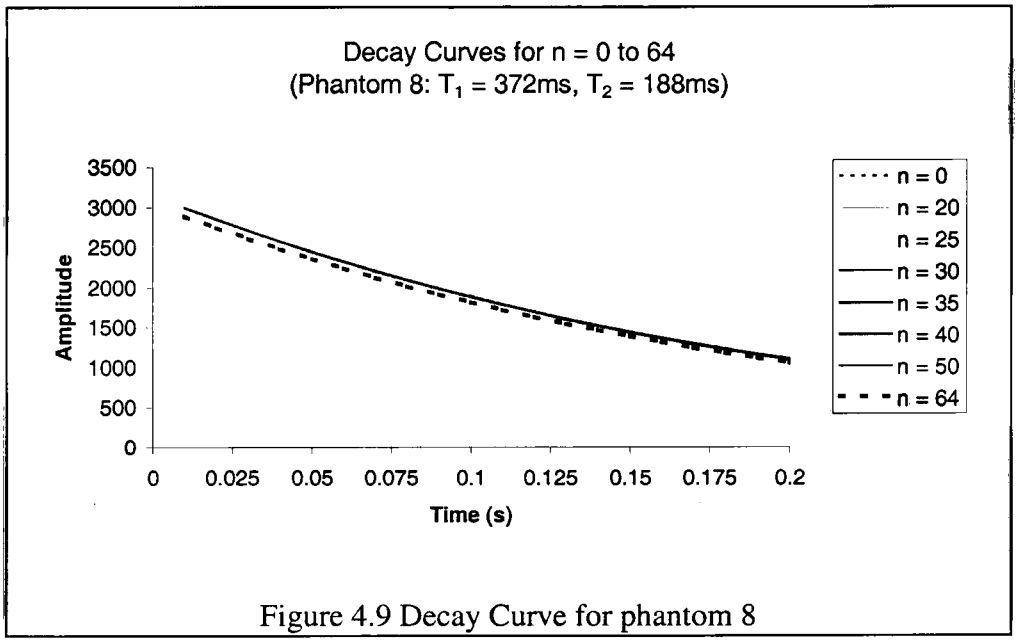

Figure 4.9 Decay Curve for phantom 8

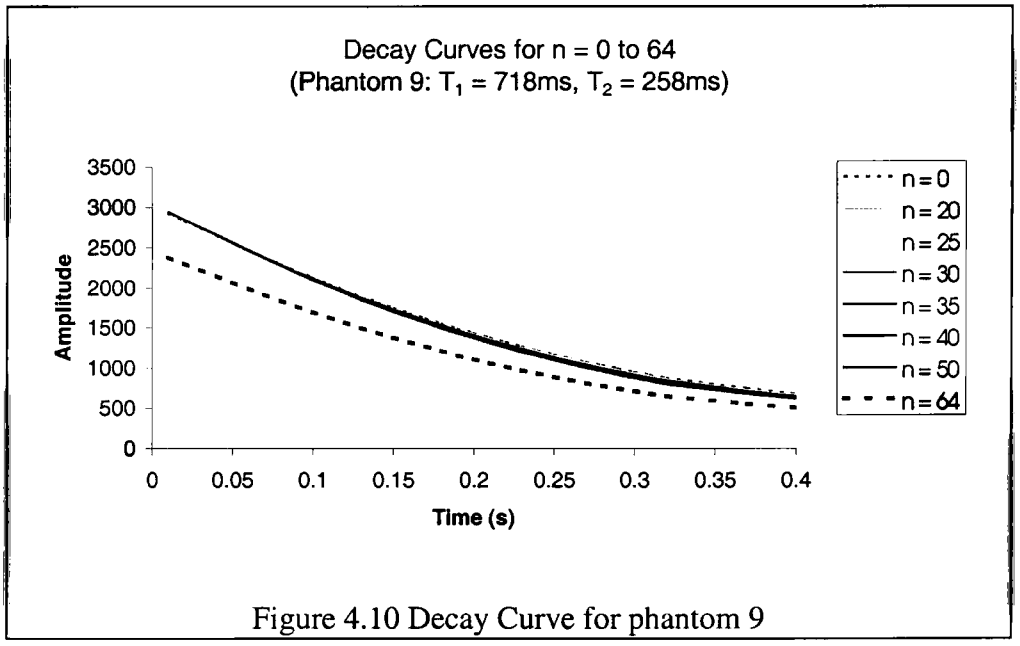

Figure 4.10 Decay Curve for phantom 9

4.4.3 Density

The density of the hydrogen nuclei of each phantom was investigated as a function of n. Figure 4.11 shows how density varied in each phantom.

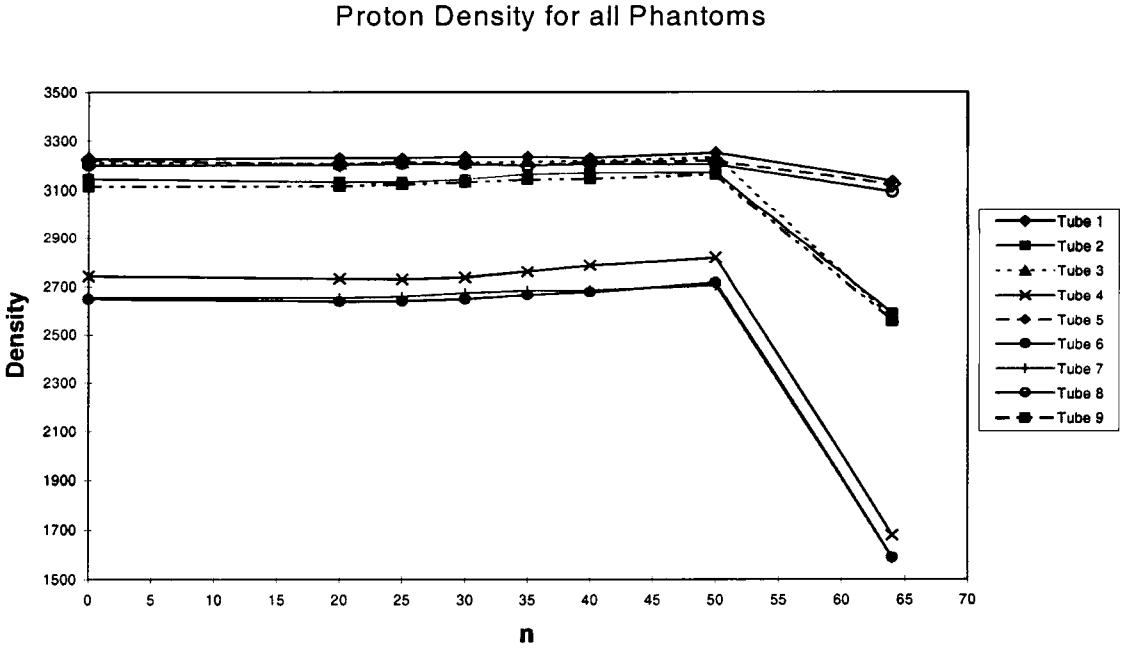

Figure 4.11 Density of each phantom as a function of n

4.4.4 Geometric Mean T_2 Relaxation

The geometric mean T_2 (GMT2) relaxation for each phantom was calculated as a function of n. Figure 4.12 shows how the GMT2 varied with n.

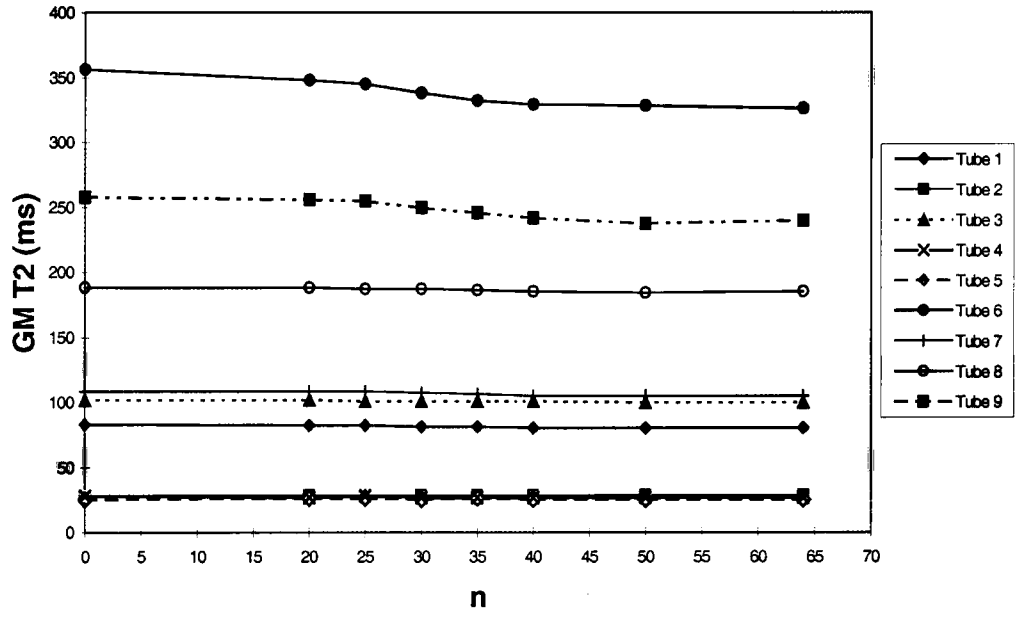

Figure 4.12 Geometric mean T2 of each phantom as a function of n

4.4.4 Chi Squared

The chi squared or degree of misfit for each phantom was calculated as a function of n. Figure 4.13 shows how the chi squared varied with n.

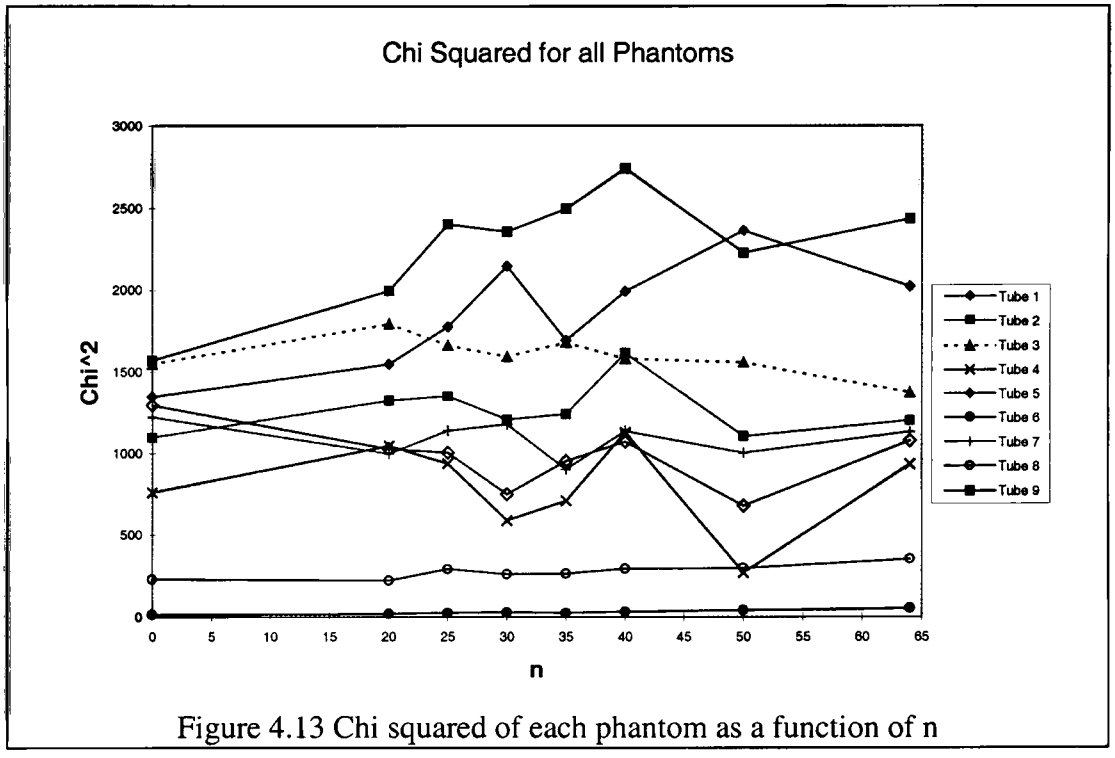

Figure 4.13 Chi squared of each phantom as a function of n

4.5 Discussion

When examining the decay curves of the nine phantoms, a change in amplitude is seen only when all lines of k-space are collected at a shorter TR. In all cases, the decay curves were exactly the same for between n = 0 and n = 50. The greatest change in signal at the short TR occurs for those phantoms with longer T_1 and T_2 relaxation times. The proton density remained virtually unchanged as n increased from 0 to 50 and then took a sharp drop at n = 64 where all of k-space is collected at the shorter TR. Likewise, the geometric mean T_2 also remain fairly constant as n ranged from 0 to 64. This indicates that collecting some regions of k-space at shorter TR values does not significantly affect the proton density and the GMT2. For phantoms with long T_2 times, there was a shift to shorter measured T_2 times at higher n values. This is not understood. A new pulse sequence with larger gradient killers at the sequence end is being prepared in order to investigate this further. The chi squared fluctuated rather wildly as the number of lines

collected at a shorter TR increased. In some cases the chi squared increased, while for others the chi squared decreased.

4.6 Conclusions

By studying samples with known T_1 and T_2 relaxation times, we were able to investigate the reliability of the variable TR pulse sequence. Comparing decay curves showed no difference between n = 0 and n = 50 – it was only when all 128 lines of k-space were collected at the shorter TR that a decrease in amplitude of the decay curve occurred. Experiments showed that proton density, GMT2 and chi squared of the T_2 decay curve fit were primarily unaffected up to and including 100 lines of k-space collected at TR of 2120ms

Chapter 5

48 Echo Variable TR *in-vivo*

5.1 Summary

Two 48 echo CPMG experiments, one with constant TR of 3.8s and one with variable TR (n = 30, TRmin = 2.12s), were performed on five healthy, normal volunteers. Regions of interest (ROI's) were drawn for 11 different white and grey matter structures including major and minor forceps, genu and splenium of the corpus callosum, posterior internal capsules, putamen, thalamus, and caudate. The decay curves are shown for both experiments. The difference of density, geometric mean T2, fraction myelin and Chi Squared are shown for the constant and variable TR.

5.2 Introduction

After qualitatively looking at the simulated brain images (Chapter 3), and performing the 48 echo experiments on the phantoms with 10 different values for n (Chapter 4), n = 30 was determined to be the best choice as far as decrease in scan time without significant loss in image quality, or distortion of density and geometric mean T_2 or increase of chi squared. The final step was to try the MRI experiment on human brain *in-vivo*.

5.3 Methods

Five volunteers were scanned. For all MRI experiments in this chapter, the 48 echo CPMG variable TR pulse sequence described in section 4.3.2 was used. Parameters were: TR = 3800ms, TRmin = 2120ms, NEX = 4, FOV = 22cm, viewmin = 34 and viewmax = 30. All experiments were performed on a GE 1.5T scanner.

5.4 Results

5.4.1 Decay Curves

In order to investigate the differences between the variable and non-variable TR 48 echo pulse sequence *in-vivo*, the decay curves from certain regions of interest were plotted for both the constant and variable TR (n = 30) for one volunteer. Figures 5.1 to 5.7 show decay curves for some ROI's.

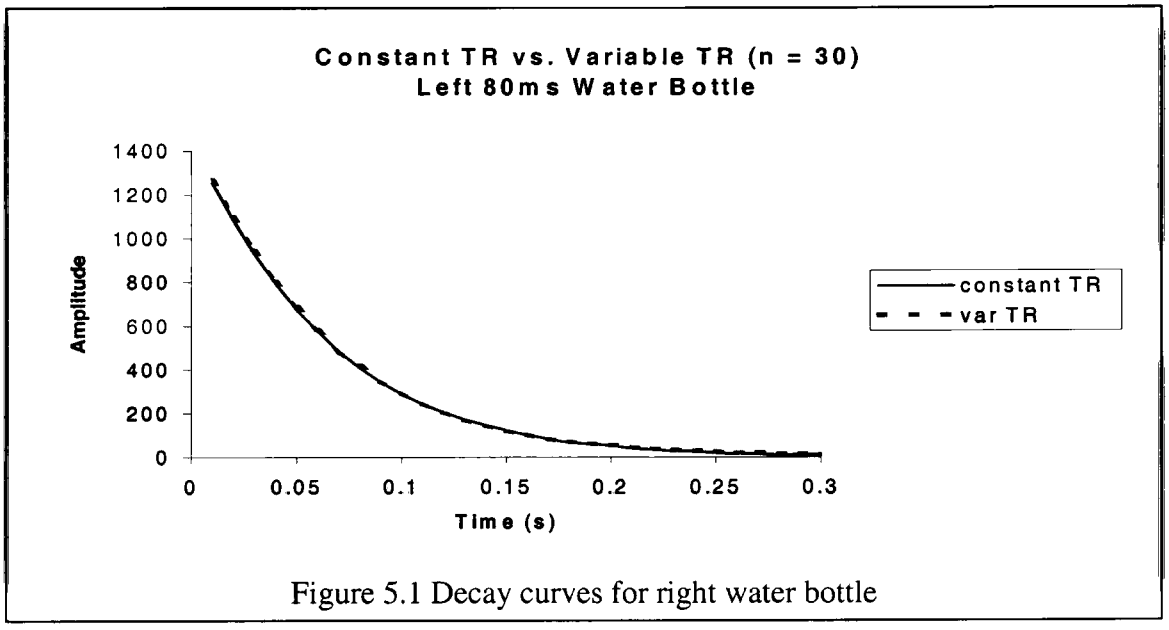

Figure 5.1 Decay curves for right water bottle

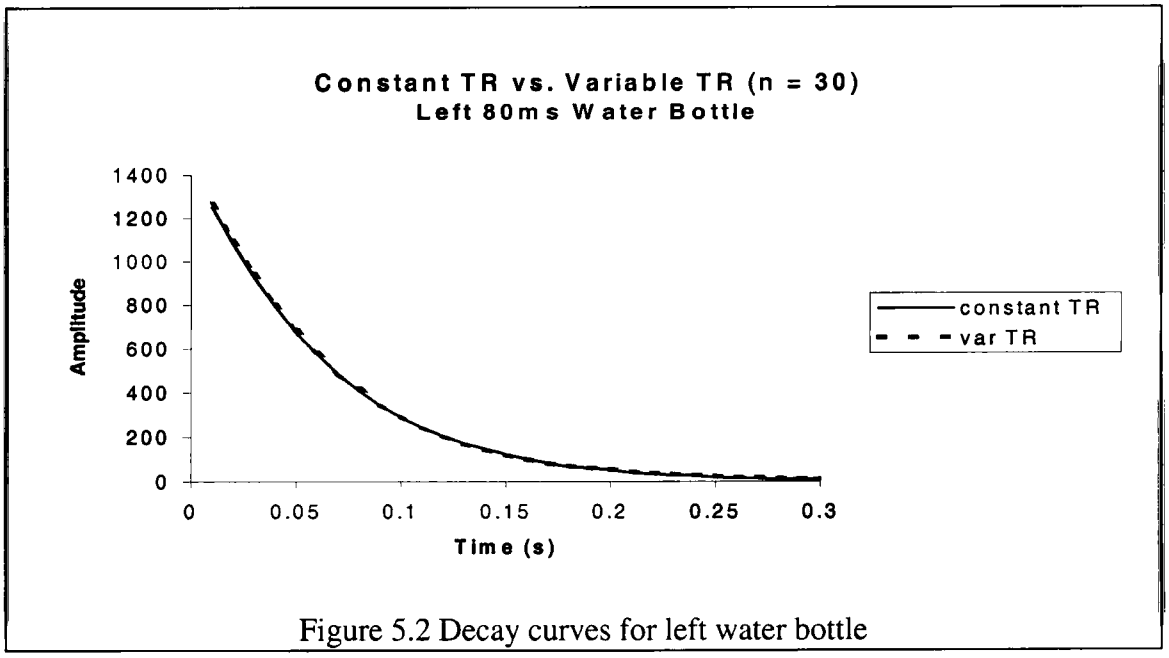

Figure 5.2 Decay curves for left water bottle

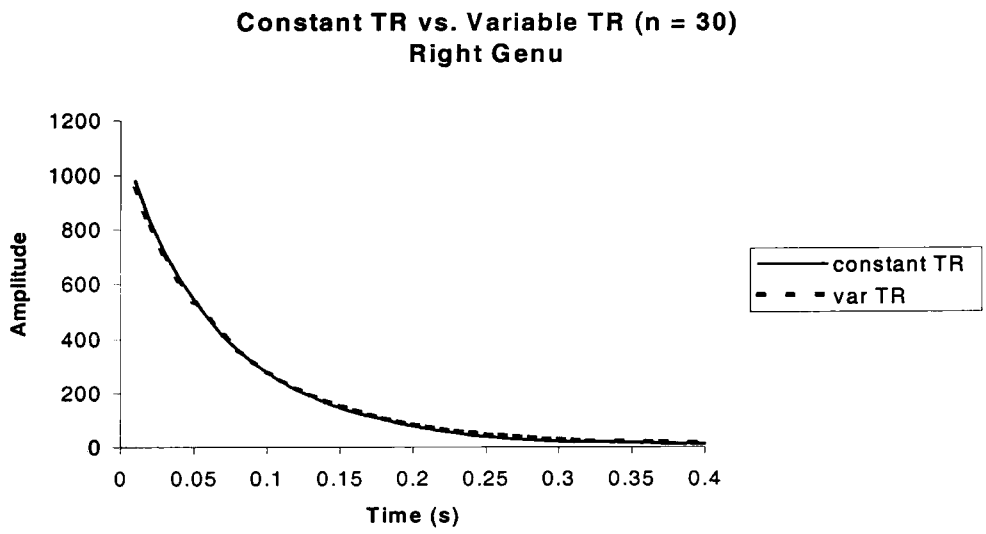

Figure 5.3 Decay curves for the right genu

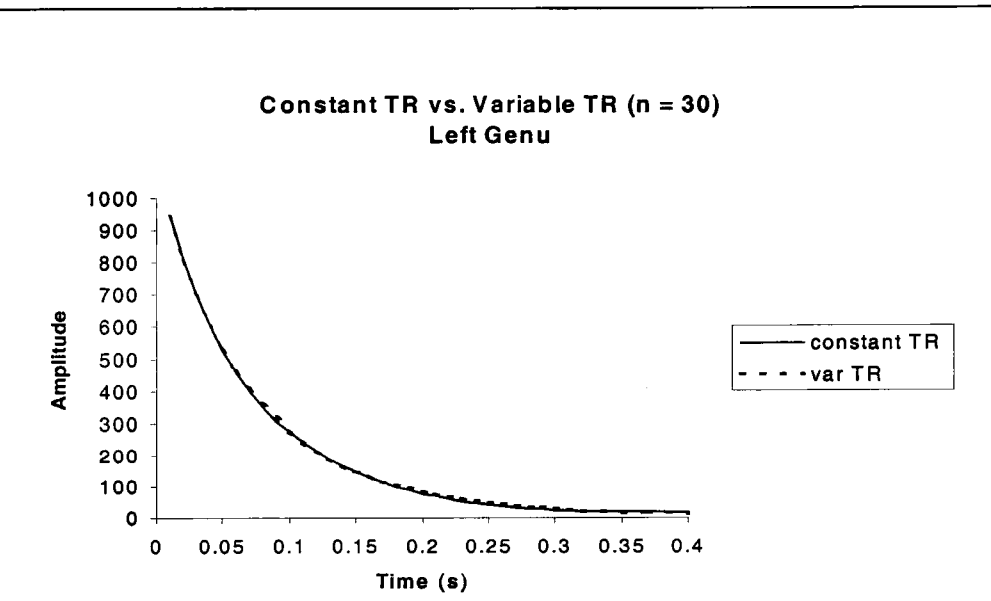

Figure 5.4 Decay curves for the left genu

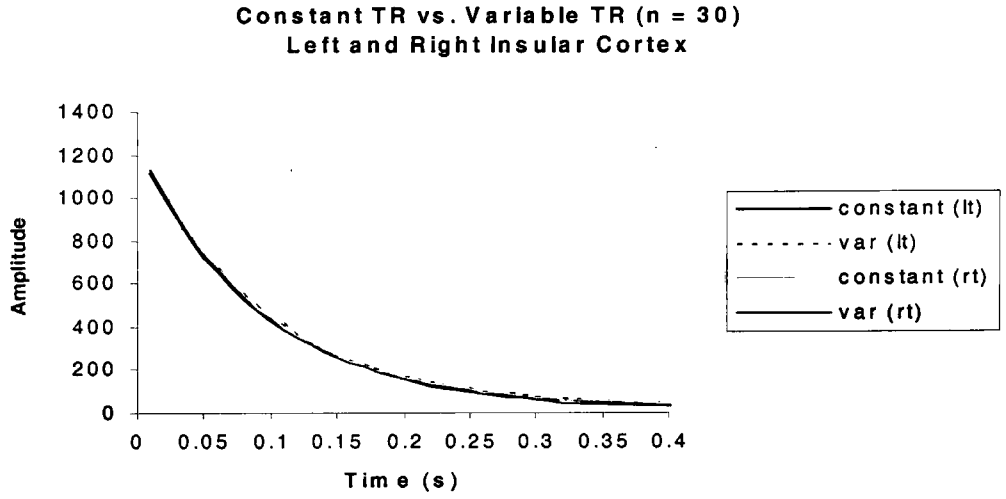

Figure 5.5 Decay curves for left and right insular cortex

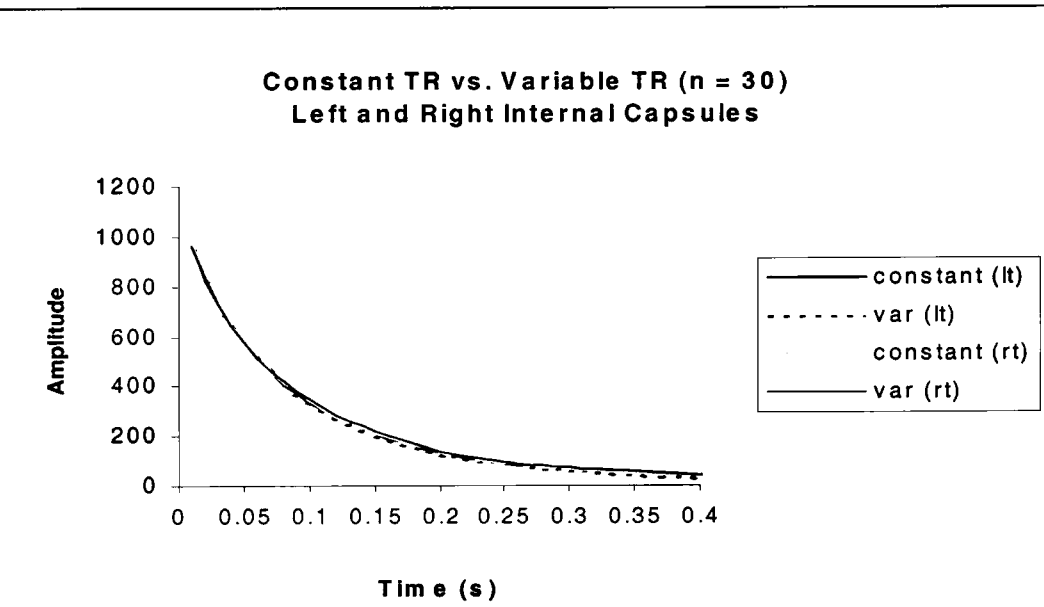

Figure 5.6 Decay curves for left and right internal capsules

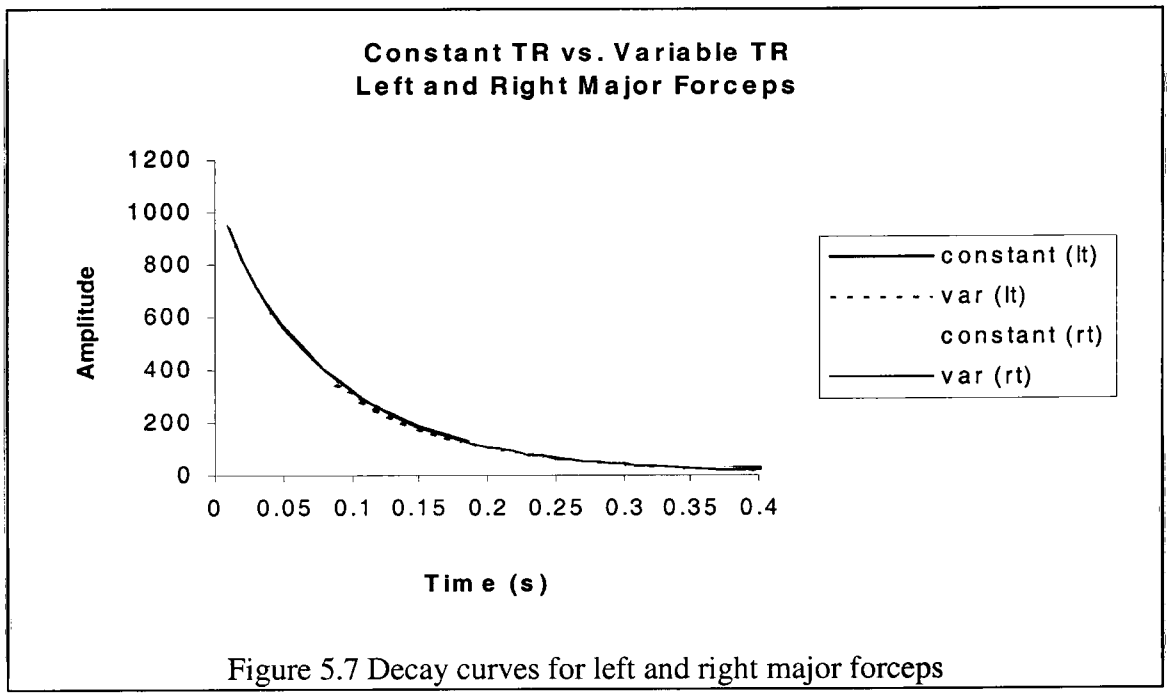

Figure 5.7 Decay curves for left and right major forceps

5.4.2 Density

As for the phantoms, the density of the hydrogen nuclei of each ROI was investigated. The proton density for the variable TR sequence was compared to the constant TR, as shown in figure 5.8.

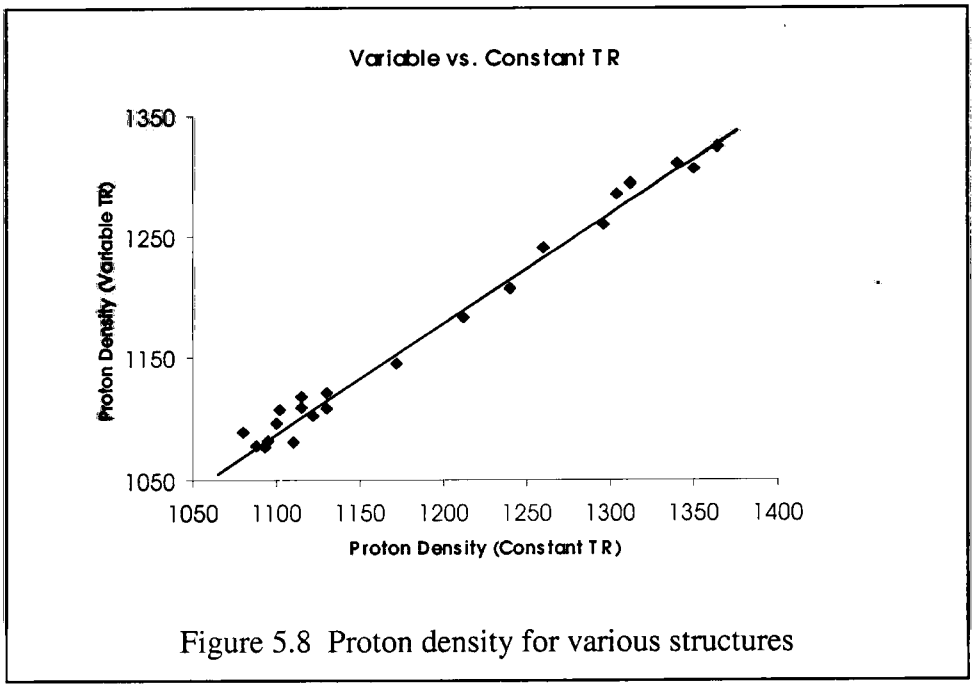

Figure 5.8 Proton density for various structures

5.4.3 Geometric Mean T_2 Relaxation

The geometric mean T_2 (GMT2) relaxation for each ROI was investigated. The comparison of GMT2 for the variable TR to the constant TR is shown in figure 5.9

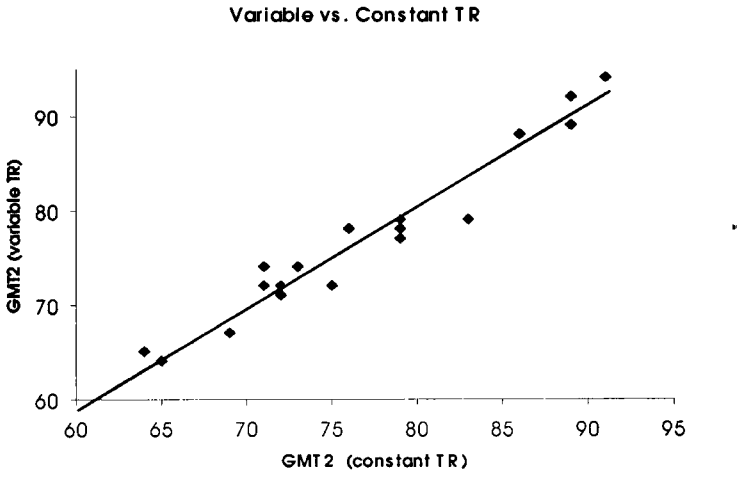

Figure 5.9 Geometric Mean T_2 for various structures

5.4.4 Fraction Myelin Water

The fraction myelin water for each ROI was investigated. The fraction myelin water for the variable TR was compared to the constant TR, as shown in figure 5.10

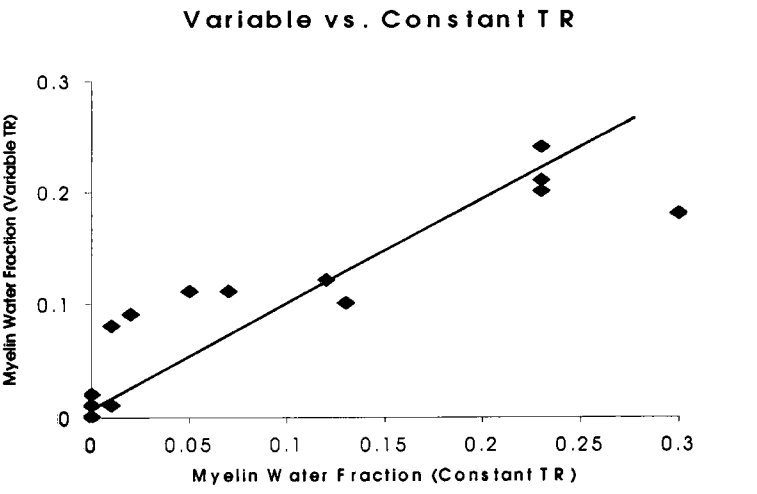

Figure 5.10 Fraction myelin water for various structues

5.4.5 Chi Squared

The chi squared or degree of misfit for each ROI was investigated. The chi squared for the variable TR was compared to the constant TR, as shown in figure 5.11

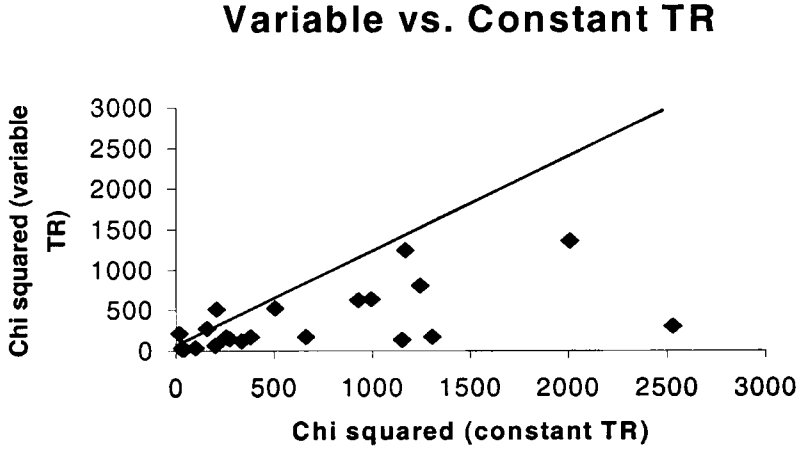

Figure 5.11 Chi squared for various structures

5.5 Discussion

When examining the decay curves of the various gray and white matter structures, no difference in amplitude is seen when comparing the constant TR with the variable TR for n = 30. In all cases, the variable and constant TR decay curves were the same. Plotting the proton density of variable to constant TR gave a linear relation, indicating that the proton density was virtually unaffected by the collecting high order regions of k-space at a shorter TR. Likewise, the geometric mean T_2 was not affected by collecting data with the variable TR sequence. Graphing the myelin water fraction from the variable TR sequence against the values obtained from the constant TR showed a fairly linear relationship. There was a greater fluctuation than for proton density and GMT2. One possible explanation is that the redrawing of the ROI's on the variable TR image was not in exactly the same place as for the constant TR. This would affect the myelin water fraction far more than the proton density or GMT2 because the myelin water signal only

makes up a small portion of the total signal. The chi squared or degree of misfit for the variable TR does not linearly corelate to the constant TR chi squared either. In fact, the chi squared is less for the variable TR. A possible explanation for this is that collecting different lines of k-space at different TR values adds smoothing to the image and reduces the amount of misfit.

5.6 Conclusion

Comparing the difference in decay curves, proton density and geometric mean T_2 showed only very minor differences between data collected using the constant TR sequence and data collected using the variable TR program in which 60 out of 128 k–space lines were collected at a shorter TR of 2120ms. Experiments showed small differences in myelin water fraction, which could be explained by ROI's being drawn slightly different on the constant and variable images. The chi squared was less for the variable TR, which could be caused by smoothing introduced when collecting different k-space lines at different TR's.

Chapter 6

Concluding Remarks

6.1 Conclusions

Simulations of the variable TR sequence, using the raw data from five T_1 weighted scans, showed that excessive blurring occurred when more than 60 out of 128 lines of k-space were collected at a shorter TR. Phantom experiments showed that proton density, GMT2 and chi squared of the T_2 decay curve fit were unaffected up to and including 100 lines of k-space collected at TR of 2120ms. Constant TR and variable TR (60 out of 128 lines at TR = 2120ms) data collected in-vivo showed only small differences in density, GMT2, fraction myelin water and χ^2 for all five volunteers.

For the 48 echo CPMG T_2 relaxation sequence, it was found that 60 lines of high order k-space could be collected at a shorter TR of 2120ms without affected image quality, proton density, GMT2, fraction myelin water and chi squared. The resulting scan time was shortened from 33 minutes to 25 minutes.

6.2 Future Work

The variation of TR across k-space that implemented for this research project can be described by figure 6.1, shown below.

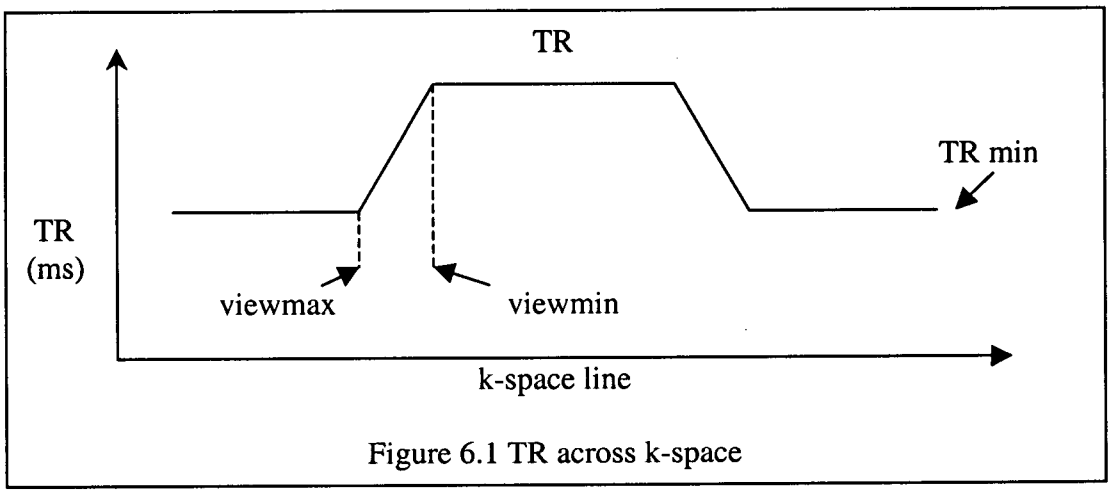

Figure 6.1 TR across k-space

There are many other k-space trajectories which could be investigated as well. One possible thing to change is the slope of the increase and decrease of k-space when moving from TRmin to TR. Figure 6.2 illustrates a possible variation where the slope is gradual.

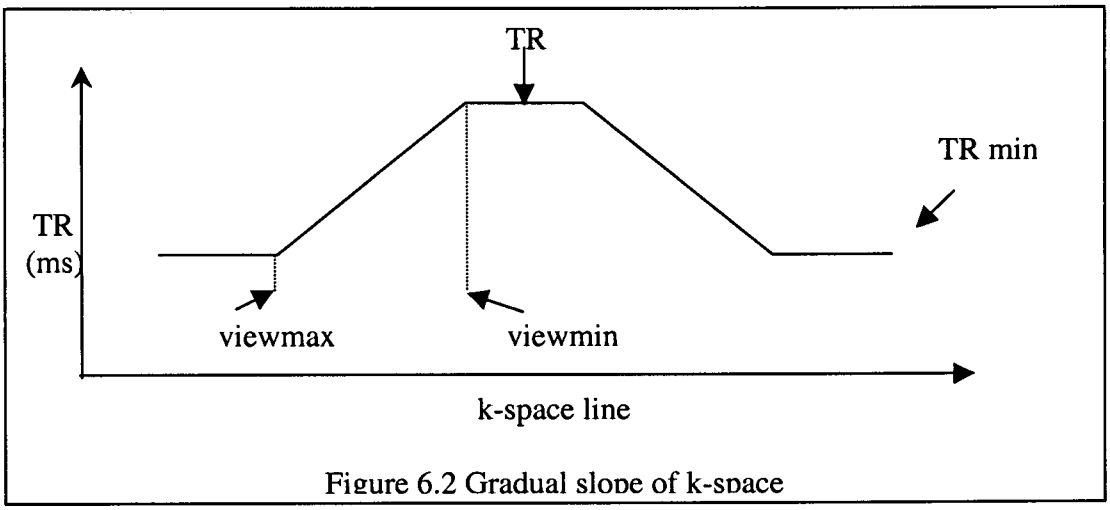

Figure 6.2 Gradual slope of k-space

Another possible modification to the k-space trajectory would be to try having TRmin much smaller than the current value of 2120ms, as shown in figure 6.3

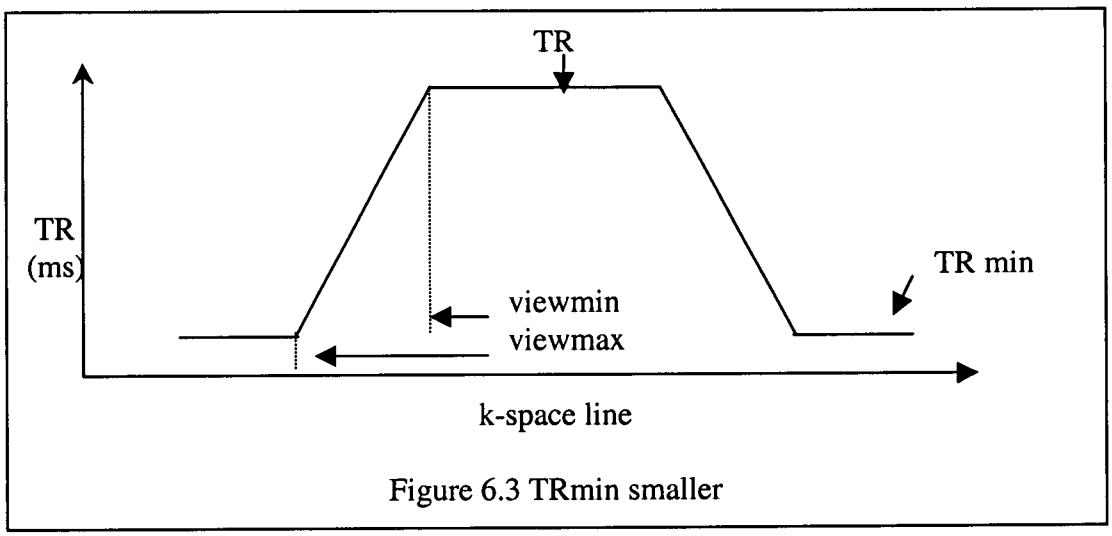

Figure 6.3 TRmin smaller

One other interesting question which has arisen for this project concerns the apparent dependence of T_2 on TR. In chapter, figure 4.12 shows that as more and more lines of k-space are collected at a shorter TR value, the geometric mean T_2 for certain phantoms (those with long T_2) decreases. This is an interesting and unexpected result and we have hypothesized one possible source of this is inaffectiveness of the killer gradient.

Appendix A

Source Code for Variable TR Simulations

MAKEV.PRO

```
; Usage   v = makeV(n, nphase, top)

FUNCTION makeV, n, nphase, top

;program to make vector V that has nphase elements ranging from
;0 to 4 which will define which TR will be used for certain
;region of k-space
;TR (ms)  Element in V
;1000                0
;1400                1
;1880                2
;2260                3
;2680                4


top = nphase - 2*n - 6

; Define zero portions of V
V = intarr(nphase)
V(0:n-1) = 0

; Define ramp up
V(n) = 1
V(n+1) = 2
V(n+2) = 3

; Top portion
V(n+3:n+top+2) = 4

; Ramp down
V(n+top + 3) = 3
V(n+top + 4) = 2
V(n+top + 5) = 1

; Not required since initialization zeroes vector V
;;V((n+top + 6):(nphase-1)) = 0

return, V
End
```

MAKE3D.PRO

```
FUNCTION make3d, f1, f2, f3, f4, f5, ctr1000, ctr1400,ctr1880,
ctr2260, ctr2680, mtr1000, mtr1400, mtr1880, mtr2260, mtr2680,
threeD


;load files

f1 = '/export/Time/BCCH/varTR2/rawdata/alex5TR/P56832'
f2 = '/export/Time/BCCH/varTR2/rawdata/alex5TR/P57344'
f3 = '/export/Time/BCCH/varTR2/rawdata/alex5TR/P57856'
f4 = '/export/Time/BCCH/varTR2/rawdata/alex5TR/P58368'
f5 = '/export/Time/BCCH/varTR2/rawdata/alex5TR/P58880'

header = bytarr(40964)

; remove header from raw data

openr, unit, f1, /get_lun
f = fstat(unit)
tr1000 = intarr(512, 128)
readu, unit, header, tr1000
free_lun, unit

openr, unit, f2, /get_lun
f = fstat(unit)
tr1400 = intarr(512, 128)
readu, unit, header, tr1400
free_lun, unit

openr, unit, f3, /get_lun
f = fstat(unit)
tr1880 = intarr(512, 128)
readu, unit, header, tr1880
free_lun, unit

openr, unit, f4, /get_lun
f = fstat(unit)
tr2260 = intarr(512, 128)
readu, unit, header, tr2260
free_lun, unit

openr, unit, f5, /get_lun
f = fstat(unit)
tr2680 = intarr(512, 128)
readu, unit, header, tr2680
free_lun, unit

; separate real and imaginary parts
```

```
rtr1000 = tr1000(indgen(256L)*2, *)
itr1000 = tr1000(indgen(256L)*2 +1, *)

rtr1400 = tr1400(indgen(256L)*2, *)
itr1400 = tr1400(indgen(256L)*2 +1, *)

rtr1880 = tr1880(indgen(256L)*2, *)
itr1880 = tr1880(indgen(256L)*2 +1, *)

rtr2260 = tr2260(indgen(256L)*2, *)
itr2260 = tr2260(indgen(256L)*2 +1, *)

rtr2680 = tr2680(indgen(256L)*2, *)
itr2680 = tr2680(indgen(256L)*2 +1, *)

; add zeros in vertical direction

rtr1000z = intarr(256, 256)
rtr1000z(*, 64:191) = rtr1000
itr1000z = intarr(256, 256)
itr1000z(*, 64:191) = itr1000

rtr1400z = intarr(256, 256)
rtr1400z(*, 64:191) = rtr1400
itr1400z = intarr(256, 256)
itr1400z(*, 64:191) = itr1400

rtr1880z = intarr(256, 256)
rtr1880z(*, 64:191) = rtr1880
itr1880z = intarr(256, 256)
itr1880z(*, 64:191) = itr1880

rtr2260z = intarr(256, 256)
rtr2260z(*, 64:191) = rtr2260
itr2260z = intarr(256, 256)
itr2260z(*, 64:191) = itr2260

rtr2680z = intarr(256, 256)
rtr2680z(*, 64:191) = rtr2680
itr2680z = intarr(256, 256)
itr2680z(*, 64:191) = itr2680

; create complex array with real and imaginary parts of k-space

ctr1000 = complex(rtr1000z, itr1000z)
ctr1400 = complex(rtr1400z, itr1400z)
ctr1880 = complex(rtr1880z, itr1880z)
ctr2260 = complex(rtr2260z, itr2260z)
ctr2680 = complex(rtr2680z, itr2680z)

; making the image
```

```
ctr1000image = fft(ctr1000, 1)
ctr1400image = fft(ctr1400, 1)
ctr1880image = fft(ctr1880, 1)
ctr2260image = fft(ctr2260, 1)
ctr2680image = fft(ctr2680, 1)

; absolute value of image and other corrections

mtr1000 = abs(ctr1000image)
mtr1000 = shift(mtr1000, 128, 128)
mtr1000 = rotate(mtr1000, 3)

mtr1400 = abs(ctr1400image)
mtr1400 = shift(mtr1400, 128, 128)
mtr1400 = rotate(mtr1400, 3)

mtr1880 = abs(ctr1880image)
mtr1880 = shift(mtr1880, 128, 128)
mtr1880 = rotate(mtr1880, 3)

mtr2260 = abs(ctr2260image)
mtr2260 = shift(mtr2260, 128, 128)
mtr2260 = rotate(mtr2260, 3)

mtr2680 = abs(ctr2680image)
mtr2680 = shift(mtr2680, 128, 128)
mtr2680 = rotate(mtr2680, 3)

;making the whole thing into 1 big 3d vector !!!!

threeD = complexarr(256, 256, 5)
threeD(*, *, 0) = ctr1000
threeD(*, *, 1) = ctr1400
threeD(*, *, 2) = ctr1880
threeD(*, *, 3) = ctr2260
threeD(*, *, 4) = ctr2680

return, threeD
End
```

MAKEVARIMAGE.PRO

```
FUNCTION makevarimage, V, threeD, rawvarTR, imagevarTR,
magvarTR, n, top, time

; this program creates variable TR images which has the first n
; lines of k space at TR = 1000ms, ramps up and then has 128 -
; 2*n - 6 lines at TR = 2680ms

; creating the complex array which will hold of the raw data

rawvarTR = complexarr(256, 256)

; pulling the correct lines out of the raw data files using V

tr1000lines = where(V eq 0)
tr1000lines = tr1000lines + 64
rawvarTR(*, tr1000lines) = threeD(*, tr1000lines, 0)

tr1400lines = where(V eq 1)
tr1400lines = tr1400lines + 64
rawvarTR(*, tr1400lines) = threeD(*, tr1400lines, 1)

tr1880lines = where(V eq 2)
tr1880lines = tr1880lines + 64
rawvarTR(*, tr1880lines) = threeD(*, tr1880lines, 2)

tr2260lines = where(V eq 3)
tr2260lines = tr2260lines + 64
rawvarTR(*, tr2260lines) = threeD(*, tr2260lines, 3)

tr2680lines = where(V eq 4)
tr2680lines = tr2680lines +64
rawvarTR(*, tr2680lines) = threeD(*, tr2680lines, 4)

;making the image

imagevarTR = fft(rawvarTR, 1)

;absolute value and other corrections

magvarTR = abs(imagevarTR)
magvarTR = shift(magvarTR, 128, 128)
magvarTR = rotate(magvarTR, 3)
tvscl, magvarTR

time = (n*2*2.12 + top*3.8 + 17.80)*4/60
print, time
return, magvarTR
End
```